

# 2.5-D Time-Domain Seismic Wavefield Modeling in Heterogeneous Viscoelastic and Tilted Transversely Isotropic Media (2023)

Moosoo Won<sup>✉</sup>, Bing Zhou, Xu Liu, Mohamed Jamal Zemerly<sup>✉</sup>, Senior Member, IEEE,  
Mohammad Al-Khaleel<sup>✉</sup>, and Mohamed Kamel Riahi<sup>✉</sup>

**Abstract**—Accurately modeling seismic wave propagation in complex subsurface structures is not only helpful to understanding seismic data and rock properties but also the fundamental part of seismic full waveform inversion to image subsurface geological structure. 3-D seismic wave modeling is often expensive due to the huge consumption of computer resources. Alternatively, an efficient and accurate 2.5-D wave modeling can be employed for obtaining the 3-D wavefield in a 2-D geological model that is often encountered in practice. We present two advanced numerical methods for the 2.5-D viscoelastic anisotropic wave modeling by integrating three innovations. First, we formulate the 2.5-D viscoelastic anisotropic wave equations, particularly for a heterogeneous tilted transversely isotropic (TTI) medium that represents many sedimentary and igneous rocks of the subsurface. Second, we extend the common memory variable method and propose a new generalized recursive convolution (RC) method to the 2.5-D wave modeling. Third, we demonstrate the real-domain fully parallelized computing of the two methods to gain high computational efficiency of wave modeling. Our calibration experiments validate the accuracy of the proposed methods, and our modeling of a benchmark geological model exhibits the capability of the proposed methods to simulate the 3-D wavefield in a complex 2-D heterogeneous viscoelastic anisotropic medium. Such robust numerical simulations may enhance the characterization of seismic wave propagation and high-resolution subsurface imaging through full-waveform inversion, which is applicable for seismic exploration, the seismological study of the earth’s interior, and geohazard detection.

**Index Terms**—2.5-D modeling, seismic waves, wave attenuation, wave propagation, wavenumber domain.

Manuscript received 14 July 2023; revised 15 September 2023; accepted 18 October 2023. Date of publication 16 November 2023; date of current version 30 November 2023. (*Corresponding author: Moosoo Won*)

Moosoo Won and Bing Zhou are with the Department of Earth Sciences, Khalifa University of Science and Technology, Abu Dhabi, United Arab Emirates (e-mail: 100058280@ku.ac.ae; bing.zhou@ku.ac.ae).

Xu Liu is with the College of Petroleum Engineering and Geosciences, King Fahd University of Petroleum and Minerals, Dhahran 31261, Saudi Arabia (e-mail: xu.liu@kfupm.edu.sa).

Mohamed Jamal Zemerly is with the Department of Electrical Engineering and Computer Science, Khalifa University of Science and Technology, Abu Dhabi, United Arab Emirates (e-mail: jamal.zemerly@ku.ac.ae).

Mohammad Al-Khaleel is with the Department of Mathematics, Khalifa University of Science and Technology, Abu Dhabi, United Arab Emirates, and also with the Department of Mathematics, Yarmouk University, Irbid 21163, Jordan (e-mail: mohammad.alkhaleel@ku.ac.ae).

Mohamed Kamel Riahi is with the Department of Mathematics, Khalifa University of Science and Technology, Abu Dhabi, United Arab Emirates (e-mail: mohamed.riahi@ku.ac.ae).

Digital Object Identifier 10.1109/TGRS.2023.3333544

## I. INTRODUCTION

THE Earth media simultaneously have both velocity anisotropy and anelastic properties [1], [2], [3]. Seismic data are influenced by the velocity anisotropy caused by subsurface structures, such as oriented fractures, minerals, and thin layers, which are often smaller than the seismic wavelength. Additionally, pores, joints, and fluid-filled cracks in rocks induce wave phase dispersion and wave energy attenuation [4], [5], [6], all of which are quantified by the quality factor ( $Q$ -factor) representing the energy loss per wave cycle and depending on the rock porosity, permeability, and fluid saturation [7]. These physical properties of rocks are simulated by a set of relaxation mechanisms [8], which can define both frequency-independent and frequency-dependent  $Q$ -factors within a frequency band. Simulating and analyzing the dispersion and attenuation in the earth media is crucial for characterizing rock properties, compensating the wave energy dissipation to seismic data, and producing a high spatial resolution image of the subsurface through seismic migration and full-waveform inversion [3], [9].

3-D seismic wave modeling involves full discrete wavefield vectors in a 3-D space, which often requires significant computer resources. While 2-D wave modeling has gained popularity due to its low computational cost, it relies on a line source that is not realistic in practice [10]. Due to the unrealistic dynamic characteristics of the 2-D wavefield of a line source, 2-D wave modeling is rarely suitable for the dynamical characterization of seismic data and directly applied to seismic full waveform inversion (FWI) for a high spatial image of the subsurface 2-D geological model, unless a transformation is applied to convert seismic data from practical point sources to synthetic line sources [11], [12], [13], [14]. To approach reality more closely, the 2.5-D wave modeling incorporates the practical point sources within a 2-D geological model and offers a more accurate 3-D wavefield than the common 2-D seismic wave modeling. Many researchers have made their contributions to the 2.5-D wave modeling [13], [14], [15], [16], [17], [18], but they focused on acoustic or viscoacoustic, elastic anisotropic, or viscoelastic isotropic media. Recently, Yang et al. [19], [20] presented the 2.5-D frequency-domain viscoelastic anisotropic wave modeling and its application to the transformation of seismic spectral data from a point source to a line source. Nonetheless, their approach faces significant

limitations in producing synthetic seismograms due to the computationally intensive nature of handling all frequency samples. Consequently, there exists a need for a 2.5-D time-domain viscoelastic anisotropic wave modeling method that can efficiently generate synthetic seismograms. Unfortunately, such 2.5-D wave modeling has not yet been observed in existing literature.

In general, the time-domain stress-strain relations in a viscoelastic rock are given by temporal convolutions, which are crucial parts of the time-domain viscoelastic anisotropic wave modeling [19] and often require significant computations [21]. Carcione et al. [22] developed the so-called memory variable method to replace the convolutions with auxiliary partial differential equations (PDEs), and then solve these auxiliary PDEs and wave equations simultaneously. This method avoids the direct computation of the convolutions and has been widely adopted for 2-D and 3-D viscoacoustic and viscoelastic wave modeling [23], [24], [25], [26], [27], [28], [29], but done nothing to the 2.5-D wave simulation.

Alternatively, Zhu and Harris [30] replace the convolutions with the fractional derivatives under the assumption of the frequency-independent  $Q$ -factors and establish the decoupled fractional Laplacian (DFL) wave equation for viscoacoustic wave modeling. The DFL method describes the wave dispersion and attenuation by two fractional terms, which is attractive to stabilize the attenuation compensation for reverse time migration. Also, using fast Fourier transform to calculate fractional Laplacians does not require the previous wavefields. Sun et al. [31] apply the low-rank one-step algorithm for the DFL method. He directly approximates the mixed-domain DFL in terms of the temporal accuracy and stability in heterogeneous media. Yang and Zhu [32] showed that the DFL equations can be achieved by using a 2nd-order polynomial and a pseudo-differential operator for the wave dispersion and dissipation, respectively, and facilitate the amplitude compensation for reverse time migration. It also explicitly incorporates the  $Q$ -factors and simplify the gradient computation of the misfit function for viscoacoustic FWI. However, solving these DFL equations involves the complex-valued variables and spends three times of the computation cost of the conventional acoustic solvers. This is critical to 3-D problem [33]. In addition, the DFL method employs the frequency-independent or average  $Q$ -factors, which faces the challenge to deal with the frequency-dependent and highly heterogeneous  $Q$ -factors [34].

Luebbers et al. [35] proposed a simple recursive formula for directly calculating the temporal convolutions rather than solving the auxiliary PDEs. However, their method assumed a constant wavefield within each time step. Kelley and Luebbers [36] introduced the piecewise linear recursive convolution (PL-RC) method for the electromagnetic wave modeling in dispersive media. Cheng et al. [37] showed an example of the PL-RC method for the time-domain 1-D viscoacoustic wave modeling. Bielak et al. [38] applied the first-order backward differences for the recursive convolutions (RC) and demonstrated 3-D viscoelastic isotropic wave modeling. Recently, Zhou et al. [39] applied the trapezoidal rule to the recursive convolution (TR-RC) and showed the successes

of 2-D viscoacoustic and viscoelastic isotropic wave modeling. Jin et al. [40] applied the Taylor series approximation to the RC, and theoretically proved its offering the best accuracy of all the RC methods and traditional memory variable method without increase of computation. Such an accurate RC method is expected to be extended to the 2.5-D viscoelastic anisotropic wave modeling.

A viscoelastic transversely isotropic medium with a tilted symmetry axis (viscoelastic tilted transversely isotropic (TTI) medium) is a common scenario in the subsurface [41] because the minerals, thin layers, joints, and fractures or cracks in rocks may align in a dip angle. If the symmetry axis or dip angle is vertical or  $90^\circ$ , the rock becomes a viscoelastic vertically transverse isotropic (VTI) medium. Many sedimentary and igneous rocks are considered viscoelastic VTI or TTI media [41], such as clay, shale, sandstone, limestone, and peridotite [42]. Zhu and Tsvankin [43] applied the Thomsen-style parameters for studying plane-wave attenuation in a viscoelastic VTI medium. Since then, such viscoelastic VTI media have been tackled with 2-D and 3-D finite difference methods [44] and the DFL method [2], [45]. In addition, da Silva et al. [6] showed that the wave modeling in a viscoelastic TTI medium may be approximated by solving a viscoacoustic wave equation through integrating the Cauchy's equation and the Thomsen's parameters. Qiao et al. [46] applied the DFL method to solve the viscoacoustic wave equation for TTI media. Gu et al. [47] derived two viscoacoustic wave equations based on different viscoelastic mechanism models. However, we have seen nothing to be done for the 2.5-D time-domain wave modeling in heterogeneous viscoelastic TTI media, where five independent complex moduli and the dip angle are functions of not only the  $x$ - and  $z$ -coordinates but also time.

This article presents two accurate and efficient numerical methods for the 2.5-D time-domain seismic wave modeling in arbitrary viscoelastic TTI media. One is the extension of the auxiliary PDE method, and another is a new generalized RC method. We theoretically derive the 2.5-D time-domain wave equations of the two methods, and then introduce the real-domain fully parallel computing to achieve high computational efficiency of the two methods for the 2.5-D viscoelastic anisotropic wave modeling. After that, we show our calibration experiments using homogeneous viscoelastic VTI and TTI models and their analytic solutions to compare the accuracies of the proposed methods. We also give our modeling experiments of two benchmark geological models: BP2007-VTI and BP2007-TTI in the elastic- and viscoelastic scenarios to show the capability of the proposed methods. Finally, we draw conclusions regarding the effectiveness and applicability of the proposed method.

## II. METHODOLOGY

### A. Viscoelastic Anisotropic Media

Earth media can be considered as the compound media that consists of elastic isotropic and viscoelastic anisotropic rocks,

in which the stress ( $\sigma_{ij}$ )-strain ( $\varepsilon_{kl}$ ) relation, often known as the constitutive equations of a medium are given by the temporal convolutions with the rock moduli ( $c_{ijkl}$ ) [4], [29], [44], [48]

$$\sigma_{ij}(\mathbf{x}, t) = c_{ijkl} * \dot{\varepsilon}_{kl} = \dot{c}_{ijkl} * \varepsilon_{kl}. \quad (1)$$

Here, the dot “.” over the variables stands for the temporal derivative, the subscripts  $\{i, j, k, l\}$  take the spatial coordinates ( $x, y, z$ ) individually, and the summation convention of the repeated subscripts is applied. The moduli  $c_{ijkl}$  is often expressed by a parallel combination of  $L$  either standard linear solids (SLSs) or Maxwell solids [26] to define a viscoelastic anisotropic rock [6]

$$c_{ijkl}(t) = c_{ijkl}^{(R)} \left[ 1 - \frac{1}{L} \sum_{\gamma=1}^L \left( 1 - \frac{\tau_{ijkl}^{(\varepsilon\gamma)}}{\tau_{ijkl}^{(\sigma\gamma)}} \right) e^{-t/\tau_{ijkl}^{(\sigma\gamma)}} \right] H(t). \quad (2)$$

Here,  $c_{ijkl}^{(R)}$  is the elastic moduli and  $\tau_{ijkl}^{(\varepsilon\gamma)}$  and  $\tau_{ijkl}^{(\sigma\gamma)}$  are the strain and stress relaxation times of the  $\gamma$ th SLS-body [6], [49]. In (2), the summation convention of the repeated subscripts is not used. Since the symmetries of strain and stress in (1), the moduli have  $c_{ijkl} = c_{jikl} = c_{ijlk} = c_{klij}$ , (2) gives 21 independent moduli defined by  $L \times 21$  strain relaxation times  $\tau_{ijkl}^{(\varepsilon\gamma)}$  and  $L \times 21$  stress relaxation times  $\tau_{ijkl}^{(\sigma\gamma)}$ .  $H(t)$  is the Heaviside step function. According to the definition of  $Q$ -factor, i.e.,  $Q^{-1}(\omega) = -\text{Im}[\tilde{c}(\omega)]/\text{Re}[\tilde{c}(\omega)]$ , one obtains

$$Q_{ijkl}^{-1}(\omega) = \frac{\sum_{\gamma=1}^L \frac{\omega/\tau^{(\sigma\gamma)} (\tau_{ijkl}^{(\varepsilon\gamma)} / \tau^{(\sigma\gamma)} - 1)}{(1/\tau^{(\sigma\gamma)})^2 + \omega^2}}{\sum_{\gamma=1}^L 1 + \frac{\omega^2 (\tau_{ijkl}^{(\varepsilon\gamma)} / \tau^{(\sigma\gamma)} - 1)}{(1/\tau^{(\sigma\gamma)})^2 + \omega^2}}. \quad (3)$$

Here, we use the assumption  $\tau_{ijkl}^{(\sigma\gamma)} = \tau^{(\sigma\gamma)}$  to reduce the number of the stress relaxation times. Unfortunately, such frequency-domain  $Q$ -factors cannot be directly applied to (2), but give a formula to determine all the relaxation times  $\{\tau_{ijkl}^{(\varepsilon\gamma)}, \tau^{(\sigma\gamma)}\}$  with the known  $Q$ -factors  $\{Q_{ijkl}(\omega_v)\}$ ,  $v = 1, 2, \dots, N\}$  through an optimization algorithm [25], [50], [51]. The known  $Q$ -factors  $\{Q_{ijkl}(\omega_v)\}$  may be either frequency-independent or frequency-dependent in a frequency band, so that (2) determined through (3) is applicable for any attenuation rock. After obtaining all these relaxation times  $\{\tau_{ijkl}^{(\varepsilon\gamma)}, \tau^{(\sigma\gamma)}\}$ , we use (2) to define a viscoelastic anisotropic medium. Apparently, as  $L = 0$ , (2) becomes the constitutive equation for elastic anisotropic rocks.

## B. 2-D and 3-D Wave Equations

The motion equation is given by [4]

$$\rho \ddot{v}_j = \sigma_{ij,i} + f_j \quad (4)$$

where  $\rho$  is density and  $f_j$  and  $v_j$  are the  $j$ th components of a body force and the particle velocity vector in the medium, respectively. The subscript, “ $i$ ” means the spatial derivative

with respect to the  $i$ th coordinate. By taking the temporal derivative to (1) gives

$$\dot{\sigma}_{ij}(\mathbf{x}, t) = \dot{c}_{ijkl} * \dot{\varepsilon}_{kl} = \dot{c}_{ijkl} * v_{k,l}. \quad (5)$$

Here,  $v_{k,l} = \partial v_k / \partial x_l$  is the derivative of the  $k$ th component of the particle velocity vector  $v$  with respect to the  $x_l$  coordinate. Substituting the temporal derivative of (2) for (5) yields

$$\dot{\sigma}_{ij}(\mathbf{x}, t) = c_{ijkl}^{(U)} v_{k,l} + \sum_{\gamma=1}^L \eta_{ij}^{(\gamma)} \quad (6)$$

where  $c_{ijkl}^{(U)} = c_{ijkl}(0)$  in (2), called the unrelaxation moduli, and  $\eta_{ij}^{(\gamma)}$  is often called as the memory variables defined by

$$\eta_{ij}^{(\gamma)}(\mathbf{x}, t) = \frac{1}{L} \left( 1 - \frac{\tau_{ijkl}^{(\varepsilon\gamma)}}{\tau^{(\sigma\gamma)}} \right) \frac{c_{ijkl}^{(R)}}{\tau^{(\sigma\gamma)}} e^{-t/\tau^{(\sigma\gamma)}} H(t) * v_{k,l}. \quad (7)$$

Equation (6) involves  $L$  temporal convolutions. Taking the temporal derivative to (7) gives the following PDEs:

$$\dot{\eta}_{ij}^{(\gamma)}(\mathbf{x}, t) = D_{ijkl}^{(\gamma)} v_{k,l} - \frac{1}{\tau^{(\sigma\gamma)}} \eta_{ij}^{(\gamma)} \quad (8)$$

where

$$D_{ijkl}^{(\gamma)} = \frac{1}{L} \left( 1 - \frac{\tau_{ijkl}^{(\varepsilon\gamma)}}{\tau^{(\sigma\gamma)}} \right) \frac{c_{ijkl}^{(R)}}{\tau^{(\sigma\gamma)}}. \quad (9)$$

Applying Voigt indexing, (8) has the matrix form

$$\begin{bmatrix} \dot{\eta}_{11}^{(\gamma)} \\ \dot{\eta}_{12}^{(\gamma)} \\ \dot{\eta}_{13}^{(\gamma)} \\ \dot{\eta}_{22}^{(\gamma)} \\ \dot{\eta}_{23}^{(\gamma)} \\ \dot{\eta}_{33}^{(\gamma)} \end{bmatrix} = \begin{bmatrix} D_{11}^{(\gamma)} & 2D_{16}^{(\gamma)} & 2D_{15}^{(\gamma)} & D_{12}^{(\gamma)} & 2D_{14}^{(\gamma)} & D_{13}^{(\gamma)} \\ D_{16}^{(\gamma)} & 2D_{66}^{(\gamma)} & 2D_{56}^{(\gamma)} & D_{26}^{(\gamma)} & 2D_{46}^{(\gamma)} & D_{36}^{(\gamma)} \\ D_{15}^{(\gamma)} & 2D_{56}^{(\gamma)} & 2D_{55}^{(\gamma)} & D_{25}^{(\gamma)} & 2D_{45}^{(\gamma)} & D_{35}^{(\gamma)} \\ D_{12}^{(\gamma)} & 2D_{26}^{(\gamma)} & 2D_{25}^{(\gamma)} & D_{22}^{(\gamma)} & 2D_{24}^{(\gamma)} & D_{23}^{(\gamma)} \\ D_{14}^{(\gamma)} & 2D_{46}^{(\gamma)} & 2D_{45}^{(\gamma)} & D_{24}^{(\gamma)} & 2D_{44}^{(\gamma)} & D_{34}^{(\gamma)} \\ D_{13}^{(\gamma)} & 2D_{36}^{(\gamma)} & 2D_{35}^{(\gamma)} & D_{23}^{(\gamma)} & 2D_{34}^{(\gamma)} & D_{33}^{(\gamma)} \end{bmatrix} \times \begin{bmatrix} v_{1,1} \\ v_{1,2} \\ v_{1,3} \\ v_{2,2} \\ v_{2,3} \\ v_{3,3} \end{bmatrix} - \frac{1}{\tau_{\sigma\gamma}} \begin{bmatrix} \eta_{11}^{(\gamma)} \\ \eta_{12}^{(\gamma)} \\ \eta_{13}^{(\gamma)} \\ \eta_{22}^{(\gamma)} \\ \eta_{23}^{(\gamma)} \\ \eta_{33}^{(\gamma)} \end{bmatrix} \quad (10)$$

which is the auxiliary PDEs for (6) and replaces (7) to avoid direct computations of the temporal convolutions. Considering all the variables and components of the vector and matrices in (4)–(10) as functions of the  $(x, z)$ - or  $(x, y, z)$ -coordinates, and the body force is either a line source  $f_j = s_j(t) \delta(x - x_s, z - z_s)$  or a point source  $f_j = s_j(t) \delta(x - x_s, y - y_s, z - z_s)$ , (4), (6), and (8) or (10) become the 2-D or 3-D viscoelastic wave equations. Here,  $s_j(t)$  and  $(x_s, y_s, z_s)$  are the  $j$ th component of the source signal and its location. Solving (4), (6), and (8) or (10) with a time-stepping scheme, such as leapfrog time-stepping [5] or the Runge–Kutta method [40], one may achieve the 2-D and 3-D viscoelastic anisotropic wave modeling. Apparently, such 2-D and 3-D viscoelastic wave modeling requires solving

the auxiliary PDEs (10). We may simply call them A-PDE method.

### C. Generalized Recursive Temporal Convolution

According to the definition of temporal convolution, (7) has the integration form

$$\eta_{ij}(t) = \int_0^t e^{-(t-\tau)/\tau_\sigma} D_{ijkl} v_{k,l}(\tau) d\tau \quad (11)$$

which can be expressed by the following recursive expression for any small time step  $\Delta t$  [40]:

$$\begin{aligned} \eta_{ij}(t) &= e^{-\Delta t/\tau_\sigma} \eta_{ij}(t - \Delta t) \\ &\quad + \sum_{m=1}^{\infty} \alpha_m \left( \frac{\partial^{m-1} D_{ijkl} v_{k,l}}{\partial^{m-1} t} \right) \Big|_{t-\Delta t} \end{aligned} \quad (12)$$

where the coefficients are given by

$$\alpha_m = (-\tau_\sigma)^m \left[ e^{-\Delta t/\tau_\sigma} + \sum_{n=0}^{m-1} \frac{1}{n!} \left( \frac{\Delta t}{-\tau_\sigma} \right)^n \right]. \quad (13)$$

Equation (13) indicates that with given  $\{\tau_\sigma, \Delta t\}$  the coefficients  $\alpha_m$  are known and the temporal convolution may be accurately approximated by (12) as long as the temporal derivatives  $(\partial^m D_{ijkl} v_{k,l} / \partial^m t)|_{t-\Delta t}$  can be estimated. For examples, as  $v_{k,l}(t)$  is a linear function in  $[t - \Delta t, t]$ , one has  $(\partial D_{ijkl} v_{k,l} / \partial t)|_{t-\Delta t} \approx [D_{ijkl} v_{k,l}(t) - D_{ijkl} v_{k,l}(t - \Delta t)] / \Delta t$  and  $\partial^m D_{ijkl} v_{k,l} / \partial^m t = 0$  for  $\forall m \geq 2$ , and  $\alpha_1 = -\tau_\sigma(e^{-\Delta t/\tau_\sigma} + 1)$  for (12). We call this approximation the first-order Taylor-series approximation of the recursive convolution (TS1-RC). Similarly, we may have the second-order Taylor-series approximation (TS2-RC) by substitutions of  $(\partial D_{ijkl} v_{k,l} / \partial t)|_{t-\Delta t} \approx [D_{ijkl} v_{k,l}(t) - 2D_{ijkl} v_{k,l}(t - \Delta t) + D_{ijkl} v_{k,l}(t - 2\Delta t)] / \Delta t^2$  and  $\partial^m (D_{ijkl} v_{k,l}) / \partial^m t = 0$  for  $\forall m \geq 3$ , we have two coefficients  $\alpha_1 = -\tau_\sigma(e^{-\Delta t/\tau_\sigma} + 1)$  and  $\alpha_2 = \tau_\sigma^2(e^{-\Delta t/\tau_\sigma} + 1 - \Delta t/\tau_\sigma)$  for (12). Thus, basing on (12) one can construct the  $m$ -order Taylor-series approximation (TSm-RC) of the temporal convolution for high accuracy. It implies that we may directly and accurately calculate the temporal convolutions by (12) rather than solve the auxiliary PDEs (8) or (10). Jin et al. [40] have given the theoretical proofs and 2-D modeling examples of the TS1-RC and A-PDE methods, showing that the TS1-RC method offers better accuracies than the A-PDE method.

### D. Viscoelastic TTI Media

A viscoelastic TTI medium may be defined by five Voigt-notated moduli  $\{c_{1'1'}, c_{1'3'}, c_{3'3'}, c_{4'4'}, c_{6'6'}\}$  plus the polar and azimuthal angles  $\{\theta_0, \varphi_0\}$ , which specify the direction of the symmetry axis at a spatial local point. According to (2) and (9), we also have five strain relaxation times  $\{\tau_{1'1'}^{(\varepsilon\gamma)}, \tau_{1'3'}^{(\varepsilon\gamma)}, \tau_{3'3'}^{(\varepsilon\gamma)}, \tau_{4'4'}^{(\varepsilon\gamma)}, \tau_{6'6'}^{(\varepsilon\gamma)}\}$  and five quantities  $\{D_{1'1'}^{(\varepsilon\gamma)}, D_{1'3'}^{(\varepsilon\gamma)}, D_{3'3'}^{(\varepsilon\gamma)}, D_{4'4'}^{(\varepsilon\gamma)}, D_{6'6'}^{(\varepsilon\gamma)}\}$ , all of which are functions of time and coordinates and employed for the transformation from the local to the global

coordinate system, i.e.,

$$\begin{pmatrix} c_{ijkl} \\ \tau_{ijkl}^{(\varepsilon\gamma)} \\ D_{ijkl}^{(\varepsilon\gamma)} \end{pmatrix} = \begin{pmatrix} c_{i'j'k'l'} \\ \tau_{i'j'k'l'}^{(\varepsilon\gamma)} \\ D_{i'j'k'l'}^{(\varepsilon\gamma)} \end{pmatrix} e_{i'i} e_{j'j} e_{k'k} e_{l'l} \quad (14)$$

where  $c_{i'j'k'l'} \in \{c_{1'1'}, c_{1'3'}, c_{3'3'}, c_{4'4'}, c_{6'6'}\}$  and  $\tau_{i'j'k'l'}^{(\varepsilon\gamma)} \in \{\tau_{1'1'}^{(\varepsilon\gamma)}, \tau_{1'3'}^{(\varepsilon\gamma)}, \tau_{3'3'}^{(\varepsilon\gamma)}, \tau_{4'4'}^{(\varepsilon\gamma)}, \tau_{6'6'}^{(\varepsilon\gamma)}\}$  are the local moduli and relaxation times, and  $e_{i'i} = \mathbf{e}_{i'} \cdot \mathbf{e}_i$  represents the cosine between the axial directions  $\mathbf{e}_i$  and  $\mathbf{e}_{i'}$ . In the 2.5-D case, due to a 2-D geological model, these moduli and the dip angles are constants in the  $y$ -direction, and we have

$$\begin{pmatrix} \mathbf{e}_{1'} \\ \mathbf{e}_{2'} \\ \mathbf{e}_{3'} \end{pmatrix} = \begin{pmatrix} \cos \theta_0 & 0 & -\sin \theta_0 \\ 0 & 1 & 0 \\ \sin \theta_0 & 0 & \cos \theta_0 \end{pmatrix} \begin{pmatrix} \mathbf{e}_1 \\ \mathbf{e}_2 \\ \mathbf{e}_3 \end{pmatrix}. \quad (15)$$

Substituting (14) and (15) for (9), we obtain the following nonzero elements of the moduli  $c_{ijkl}$  and the components  $D_{ijkl}^{(\varepsilon\gamma)}$  in Voigt notation:

$$\mathbf{c}_{IJ} = \begin{bmatrix} c_{11} & c_{12} & c_{13} & 0 & c_{15} & 0 \\ & c_{22} & c_{23} & 0 & c_{25} & 0 \\ & & c_{33} & 0 & c_{35} & 0 \\ & & & c_{44} & 0 & c_{46} \\ & & & & c_{55} & 0 \\ & & & & & c_{66} \end{bmatrix} \quad (16)$$

and

$$\mathbf{D}_{IJ}^{(\varepsilon\gamma)} = \begin{bmatrix} D_{11}^{(\varepsilon\gamma)} & 0 & 2D_{15}^{(\varepsilon\gamma)} & D_{12}^{(\varepsilon\gamma)} & 0 & D_{13}^{(\varepsilon\gamma)} \\ 0 & 2D_{66}^{(\varepsilon\gamma)} & 0 & 0 & 2D_{46}^{(\varepsilon\gamma)} & 0 \\ D_{15}^{(\varepsilon\gamma)} & 0 & 2D_{55}^{(\varepsilon\gamma)} & D_{25}^{(\varepsilon\gamma)} & 0 & D_{35}^{(\varepsilon\gamma)} \\ D_{12}^{(\varepsilon\gamma)} & 0 & 2D_{25}^{(\varepsilon\gamma)} & D_{22}^{(\varepsilon\gamma)} & 0 & D_{23}^{(\varepsilon\gamma)} \\ 0 & 2D_{46}^{(\varepsilon\gamma)} & 0 & 0 & 2D_{44}^{(\varepsilon\gamma)} & 0 \\ D_{13}^{(\varepsilon\gamma)} & 0 & 2D_{35}^{(\varepsilon\gamma)} & D_{23}^{(\varepsilon\gamma)} & 0 & D_{33}^{(\varepsilon\gamma)} \end{bmatrix} \quad (17)$$

respectively. As  $\theta_0 = 0$  in (15), (14) reduces to a viscoelastic VTI medium. To obtain the nonzero elements  $D_{ij}^{(\varepsilon\gamma)}$  in (17), we follow two steps: 1) determine the relaxation times  $\{\tau_{i'j'k'l'}^{(\varepsilon\gamma)}, \tau^{(\varepsilon\gamma)}\}$  through optimizing (3) with given the local  $Q$ -factors  $\{Q_{1'1'}, Q_{1'3'}, Q_{3'3'}, Q_{4'4'}, Q_{6'6'}\}$  and 2) apply (14) to transform the given local moduli  $\{c_{1'1'}^{(R)}, c_{1'3'}^{(R)}, c_{3'3'}^{(R)}, c_{4'4'}^{(R)}, c_{6'6'}^{(R)}\}$ , relaxation times  $\{\tau_{1'1'}^{(\varepsilon\gamma)}, \tau_{1'3'}^{(\varepsilon\gamma)}, \tau_{3'3'}^{(\varepsilon\gamma)}, \tau_{4'4'}^{(\varepsilon\gamma)}, \tau_{6'6'}^{(\varepsilon\gamma)}\}$  and quantities  $\{D_{1'1'}^{(\varepsilon\gamma)}, D_{1'3'}^{(\varepsilon\gamma)}, D_{3'3'}^{(\varepsilon\gamma)}, D_{4'4'}^{(\varepsilon\gamma)}, D_{6'6'}^{(\varepsilon\gamma)}\}$  into the global moduli  $\{c_{ijkl}^{(R)}\}$ , relaxation times  $\{\tau_{ijkl}^{(\varepsilon\gamma)}\}$ , and matrices  $\{D_{ijkl}^{(\varepsilon\gamma)}\}$ , respectively.

### E. 2.5-D Wave Equations

Considering a point source in a 2-D geological model and applying the Fourier transform to the  $y$ -coordinate in (4) and (6), we have the gradient-operator change from  $\nabla = (\partial_x, \partial_y, \partial_z)$  into  $\bar{\nabla} = (\partial_x, ik_y, \partial_z)$ , and the 3-D wavefield  $\{v_j, \sigma_{ij}, \eta_{ij}^{(\varepsilon\gamma)}\}$  into the wavenumber ( $k_y$ )-domain wavefield

$\{\tilde{v}_j, \tilde{\sigma}_{ij}, \tilde{\eta}_{ij}^{(y)}\}$ . Equations (4), (6), (8), and (12) become

$$\begin{aligned} & \dot{\tilde{\sigma}}_{ij}(\mathbf{x}, t) \\ &= c_{ijkl}^{(U)} \tilde{v}_{k,l} + ik_y c_{ijk2}^{(U)} \tilde{v}_k + \sum_{\gamma=1}^L \tilde{\eta}_{ij}^{(\gamma)}, \\ & \quad (i, j, k = 1, 2, 3; l = 1, 3) \end{aligned} \quad (18)$$

$$\begin{aligned} \dot{\tilde{v}}_j &= \rho^{-1} (\tilde{\sigma}_{ij,i} + ik_y \tilde{\sigma}_{2j}) + f_j, \\ & \quad (i = 1, 3; j = 1, 2, 3) \end{aligned} \quad (19)$$

$$\begin{aligned} \dot{\tilde{\eta}}_{ij}^{(y)} &= D_{ijkl}^{(y)} \tilde{v}_{k,l} + ik_y D_{ijk2}^{(y)} \tilde{v}_k - \frac{1}{\tau_{\sigma y}} \tilde{\eta}_{ij}^{(y)}, \\ & \quad (i, j, k = 1, 2, 3; l = 1, 3) \end{aligned} \quad (20)$$

$$\begin{aligned} \tilde{\eta}_{ij}^{(y)}(t) &= e^{-\Delta t/\tau_{\sigma}} \tilde{\eta}_{ij}^{(y)}(t - \Delta t) \\ &+ \sum_{m=1}^{\infty} \alpha_m \left( \frac{\partial^{m-1} (D_{ijkl}^{(y)} \tilde{v}_{k,l} + D_{ijk2}^{(y)} ik_y \tilde{v}_k)}{\partial^{m-1} t} \right) \Big|_{t-\Delta t}. \end{aligned} \quad (21)$$

Equations (18) and (19) are referred to as the 2.5-D viscoelastic anisotropic wave equations, (20) is the 2.5-D version of the A-PDE method, and (21) is the 2.5-D form of the TSm-RC method. Apparently, as  $k_y = 0$ , (18)–(21) degenerate to the 2-D viscoelastic anisotropic wave equations (a line source), and the complex  $k_y$ -domain wavefield  $\{\tilde{\sigma}_{ij}, \tilde{v}_j, \tilde{\eta}_{ij}\}$  become the real wavefield  $\{\sigma_{ij}, v_j, \eta_{ij}\}$ . Therefore, (18)–(21) are valid for both the 2-D and 2.5-D viscoelastic anisotropic wave modeling. Solving either (18)–(20) (A-PDE method) or (18) and (19) with (21) (TSm-RC), one may achieve the 2.5-D viscoelastic anisotropic wave modeling. However, these solving processes are often implemented within the complex  $k_y$ -domain, which spends much more computer memory and runtimes than the common 2-D viscoelastic anisotropic wave modeling. Therefore, accurately and efficiently solving the 2.5-D viscoelastic anisotropic wave equations becomes crucial to model the 3-D wavefields in a 2-D geological model.

If the point source is located in the central plane, i.e., the  $(x, 0, z)$ -plane, the 3-D wavefield vectors and tensors  $\{v_j, \sigma_{ij}, \eta_{ij}^{(y)}\}$  exhibit symmetric or antisymmetric in terms of the source and geophone directions [52], e.g.,  $\{v_1(y), v_2(y), v_3(y)\} = \{v_1(-y), -v_2(y), v_3(-y)\}$  resulting in  $\{\tilde{v}_1, \tilde{v}_2, \tilde{v}_3\} = \{\tilde{v}_1^{(R)}, i\tilde{v}_2^{(I)}, \tilde{v}_3^{(R)}\}$ ,  $\{\tilde{\sigma}_{11}, \tilde{\sigma}_{12}, \tilde{\sigma}_{13}, \tilde{\sigma}_{22}, \tilde{\sigma}_{23}, \tilde{\sigma}_{33}\} = \{\tilde{\sigma}_{11}^{(R)}, i\tilde{\sigma}_{12}^{(I)}, \tilde{\sigma}_{13}^{(R)}, \tilde{\sigma}_{22}^{(R)}, i\tilde{\sigma}_{23}^{(I)}, \tilde{\sigma}_{33}^{(R)}\}$  and  $\{\tilde{\eta}_{11}^{(y)}, \tilde{\eta}_{12}^{(y)}, \tilde{\eta}_{13}^{(y)}, \tilde{\eta}_{22}^{(y)}, \tilde{\eta}_{23}^{(y)}, \tilde{\eta}_{33}^{(y)}\} = \{\tilde{\eta}_{11}^{(y,R)}, i\tilde{\eta}_{12}^{(y,I)}, \tilde{\eta}_{13}^{(y,R)}, \tilde{\eta}_{22}^{(y,R)}, i\tilde{\eta}_{23}^{(y,I)}, \tilde{\eta}_{33}^{(y,R)}\}$ . Here, the superscripts “ $R$ ” and “ $I$ ” stand for the real and imaginary parts of these variables. Substituting these relationships into (18)–(21), the imaginary unit “ $i$ ” is absent and the resultant 2.5-D viscoelastic wave equations become the real-domain PDEs. This implies that the time-domain 2.5-D viscoelastic anisotropic wave modeling can be implemented in the real domain for significantly saving computer memory and runtime.

#### F. Wavenumber Sampling

To obtain the 3-D wavefield  $v(t, x, y, z)$  in a 2-D geological model, the inverse Fourier transform of the  $k_y$ -domain

wavefield  $\tilde{v}(t, x, k_y, z)$  must be carried out [19], [53]. Considering the symmetry of the solution  $\tilde{v}_{sg}(t, x, k_y, z) = (-1)^{s+g} \tilde{v}_{sg}(t, x, -k_y, z)$  [18], the inverse Fourier transform becomes

$$\begin{aligned} v_{sg}(t, x, y, z) \\ \approx \frac{1}{\pi} \sum_{n=1}^{N_{ky}} w_n \tilde{v}_{sg}(t, x, k_y^{(n)}, z) \begin{cases} \cos(k_y^{(n)} y), s+g = \text{even} \\ i \sin(k_y^{(n)} y), s+g = \text{odd} \end{cases}. \end{aligned} \quad (22)$$

Here, the superscripts  $\{s, g\} = 1, 2$ , and 3 represent the source and geophone directions in the  $x$ -,  $y$ -, and  $z$ -axis,  $k_y^{(n)} \in [0, k_y^c]$  and  $k_y^c$  and  $N_{ky}$  are the cut-off wavenumber and the total number of the  $k_y$ -samples, respectively. The coefficients  $w_n = (n-1)k_y^c/(N_{ky}-1)$  ( $n = 1, 2, \dots, N_{ky}$ ) are  $N_{ky}$   $k_y$ -samples or the Gaussian quadrature weights of the abscissae  $\{k_y^{(n)}, n = 1, 2, \dots, N_{ky}\}$ . By our primary experiments, we found the optimal cut-off wavenumber

$$k_y^c \geq \frac{2.5\omega_c}{V_{\min}} \quad (23)$$

and the proper total number of the  $k_y$ -samples

$$N_{ky} \geq 1 + \text{int} \left( \frac{k_y^c (V_{\max} T + \lambda_{\max})}{2\pi} \right). \quad (24)$$

Here,  $\omega_c$ ,  $V_{\min}$ , and  $V_{\max}$  are the central frequency of the source and the minimum and maximum velocities of the medium, respectively.  $T$  and  $\lambda_{\max}$  are the total time length and the largest wavelength in the simulation. Comparing (23) and (24) with the  $k_y$ -sampling strategy given in [52], one may find that the time-domain  $k_y$ -sampling strategy quite differs from the frequency-domain  $k_y$ -sampling strategy for the firm absence of the artificial reflections due to the undersampled wavenumbers. After determining  $k_y^c$  and  $N_{ky}$ , one may employ either the regular (equal spacing) or irregular spacing (Gauss-Legendre abscissae) for the wavenumber samples  $\{k_y^{(n)}\}$  and weights  $\{w_n\}$  for (22) so as to obtain the 3-D time-domain wavefield  $v_{sg}(t, x, y, z)$ . It means that although the solving process is implemented in the real domain, (18)–(21) must be solved for  $N_{ky}$  times. Thus, either the A-PDE or TSm-RC method is still time-consuming. However, (18)–(21) show that the solving processes for different  $k_y$  samples are independent to each other, so we can accomplish the solving processes by parallel computing, i.e., we use open multi-processing (OpenMP)/message passing interface (MPI) to assign all the solving processes to  $N_{ky}$  cores on a high-performing computing facility and simultaneously solve (18)–(21), and then gather the solutions to obtain the 3-D wavefields. Such fully parallelized real-domain implementation significantly gains excellent computational efficiency for the 2.5-D time-domain viscoelastic wave modeling.

### III. NUMERICAL EXPERIMENTS

To solve the 2.5-D wave equations with A-PDE and TSm-RC methods, one must calculate the gradients  $\tilde{v}_{k,l} = \partial_l \tilde{v}_k$  and  $\tilde{\sigma}_{ij,i} = \partial_i \tilde{\sigma}_{ij}$ , as well as the temporal derivatives  $\{\dot{\tilde{v}}_j, \dot{\tilde{\sigma}}_{ij}, \dot{\tilde{\eta}}_{ij}\}$  [see (20)–(23)]. For all the numerical experiments, we apply

TABLE I  
VISCOELASTIC MODELS FOR CALIBRATION EXPERIMENTS.  
EACH MODEL HAS LOW AND HIGH ATTENUATIONS

Model ( $1 \times 1 \text{ km}^2$ )	Relaxed Moduli (GPa) and density ( $\text{kg}/\text{m}^3$ )	$Q$ -factors
VTI-1	$c_{11}^{(R)} = 12.5, c_{33}^{(R)} = 8.5, c_{44}^{(R)} = 2,$ $c_{66}^{(R)} = 4.5, c_{13}^{(R)} = -c_{44}^{(R)}, \rho = 1000$	$Q_{11} = 120, Q_{33} = 80, Q_{44} = 40,$ $Q_{66} = 60, Q_{13} = Q_{44}$
		$Q_{11} = 30, Q_{33} = 20, Q_{44} = 10,$ $Q_{66} = 15, Q_{13} = Q_{44}$
VTI-2	$c_{11}^{(R)} = 12.5, c_{44}^{(R)} = 2, c_{66}^{(R)} = 4.5,$ $c_{33}^{(R)} = c_{11}^{(R)}, c_{13}^{(R)} = c_{11}^{(R)} - 2c_{44}^{(R)},$ $\rho = 1000$	$Q_{11} = 120, Q_{44} = 40, Q_{66} = 60,$ $Q_{33} = Q_{11}, Q_{13} = Q_{11} - 2Q_{44}$
		$Q_{11} = 30, Q_{44} = 10, Q_{66} = 15,$ $Q_{33} = Q_{11}, Q_{13} = Q_{11} - 2Q_{44}$
ORT	$c_{11}^{(R)} = 12.5, c_{22}^{(R)} = 8.5, c_{33}^{(R)} = 10,$ $c_{44}^{(R)} = 2, c_{55}^{(R)} = 3, c_{66}^{(R)} = 4.5,$ $c_{13}^{(R)} = -c_{44}^{(R)}, \rho = 1000$	$Q_{11} = 120, Q_{22} = 80, Q_{33} = 100,$ $Q_{44} = 40, Q_{55} = 50, Q_{66} = 60,$ $Q_{13} = -Q_{44}$
		$Q_{11} = 30, Q_{22} = 20, Q_{33} = 25,$ $Q_{44} = 10, Q_{55} = 13, Q_{66} = 15,$ $Q_{13} = -Q_{44}$

the subdomain curvilinear Chebyshev differentiation [54] for the spatial derivatives, and the 3rd-order Adams–Bashforth explicit multistep formula for the temporal derivatives [55]. The subdomain curvilinear Chebyshev differentiation uses a proper number ( $\geq 5$ ) of the Chebyshev points in each subdomain of the irregular mesh to calculate the spatial derivatives in the wave equations and brings much higher accuracy than the common finite difference approximation due to its exponential convergence, so as to guarantee the accuracies of these differential computations. In addition, the generalized stiffness reduction method [56] is applied to absorb the artificial reflections from the edges of the computation domain, and the fully parallelized real-domain implementation using multicores is adopted to efficiently yield the numerical solutions of 3-D wavefield in all the models.

#### A. Calibration Experiment

To assess the accuracies of the proposed methods: A-PDE, TS1-RC, and TS2-RC, we employed three homogeneous anisotropic models—two VTI media (VTI-1 and VTI-2) and one orthorhombic medium (ORT), whose moduli and  $Q$ -factors are given in Table I. Each model has two sets of  $Q$ -factors representing a low and a high attenuation media. The Ricker’s wavelet with a central frequency of 30 Hz and a delay time of 0.05 s is employed as the source signal. Varyčuk [57] gave the frequency-domain analytical solutions of these three models, so that we can obtain the seismograms by carrying out the inverse Fourier transform with enough samples of the frequency-domain analytic solutions, and then calibrated the numerical solutions.

Based on the model parameters given in Table I and the source frequency, we determined the relaxation times  $\{\tau_{\epsilon\gamma}^{(ijkl)}, \tau_{\sigma\gamma}\}$  of the moduli  $c_{ijkl}$ , worked out the minimum wavelength  $\lambda_{\min} = 54$  m, the cut-off wavenumber  $k_y^c = 0.3332$ , and the number of the  $k_y$ -samples  $N_{ky} = 126$ , and then applied a  $5 \times 5$  Chebyshev points in each  $25 \times 25$  m subdomain for the Chebyshev spatial differentiations, so that the models are discretized by a  $393 \times 393$  grid (including the absorbing zone), and the points per wavelengths (PPWs) reaches 9.4. One hundred twenty-six Gauss–Legendre abscissas in  $[0, k_y^c]$  were used as the  $k_y$ -samples and 126 cores were utilized to achieve the fully parallel computing of the 2.5-D wave modeling, e.g., VTI-2 model spent about 19.2 min to

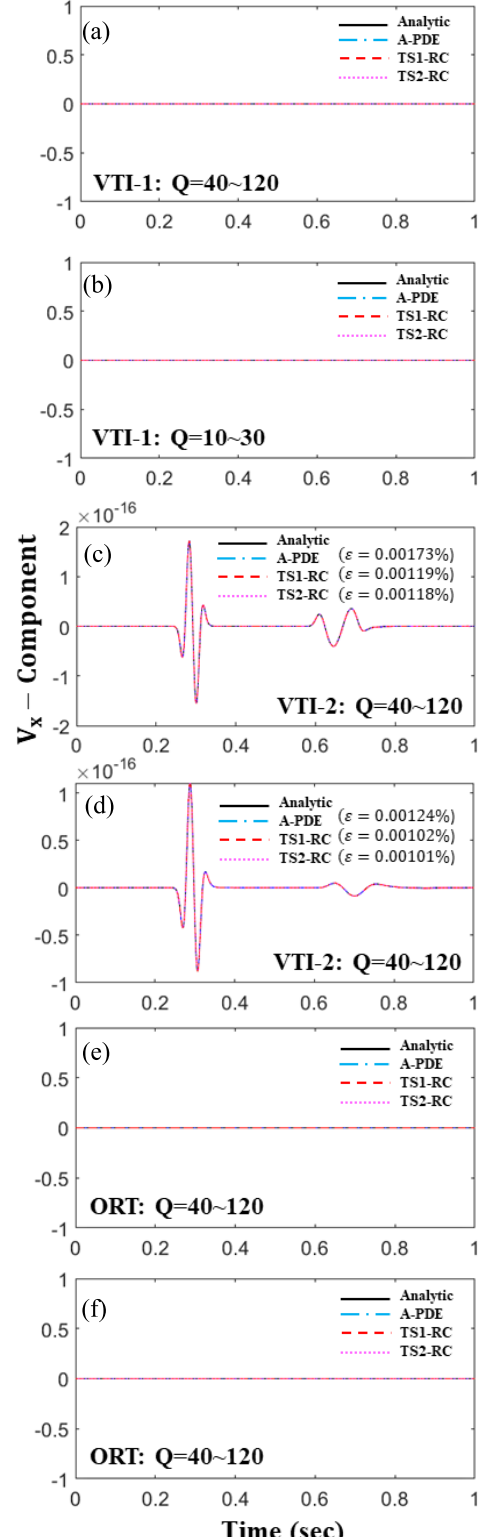


Fig. 1. Seismograms of the  $V_x$ -components yielded by three numerical methods (A-PDE, TS1-RC, and TS2-RC) and analytical method for homogeneous viscoelastic VTI-1, VTI-2, and ORT media in (a), (c), and (e) low attenuation, and (b), (d), and (f) high attenuation given in Table I.

yield the 3-D wavefield solutions, just about 1.7 times the 2-D modeling.

Figs. 1 and 2 show the  $V_x$ - and  $V_z$ -components computed by three numerical methods (A-PDE, TS1-RC, TS2-RC) and the analytical method. The root-mean-square percentage error

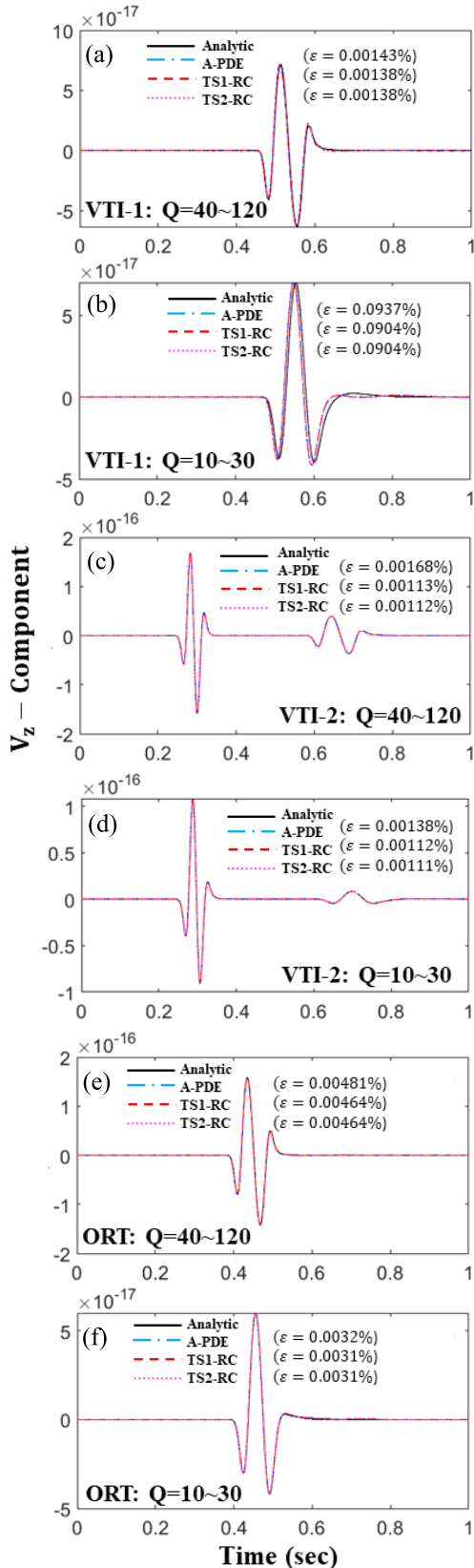


Fig. 2. Seismograms of the  $V_z$ -components yielded by three numerical methods (A-PDE, TS1-RC, and TS2-RC) and an analytical method for homogeneous viscoelastic VTI-1, VTI-2, and ORT media in (a), (c), and (e) low attenuation, and (b), (d), and (f) high attenuation given in Table I.

(RMSPE,  $\varepsilon = 100\% \times (\sum (S_{\text{numerical}}/S_{\text{analytic}} - 1)^2/n)^{1/2}$ ) between the numerical and analytical solutions are calculated

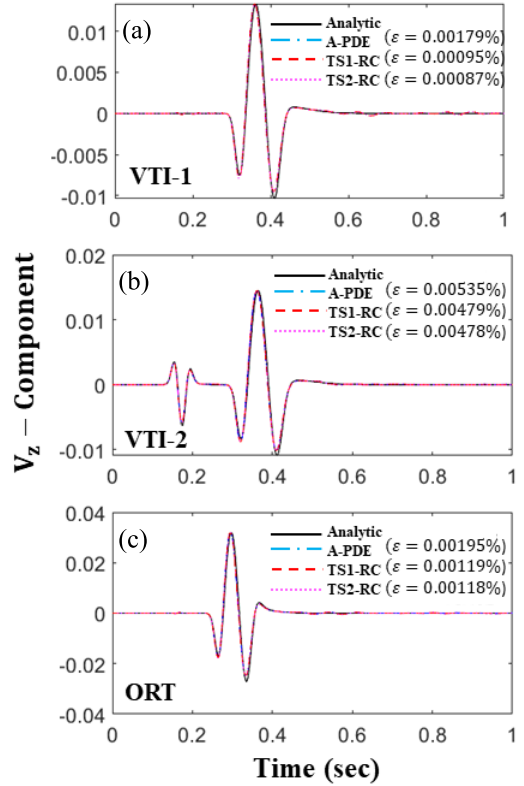


Fig. 3. Seismograms of the  $V_z$ -components yielded by three numerical methods (A-PDE, TS1-RC, TS2-RC) and analytical method for three anisotropic viscoelastic TTI media in high attenuation case, whose parameters are given in Table I: (a) VTI-1, (b) VTI-2, and (c) ORT media and the tilted angle is  $45^\circ$ .

(see the brackets in Figs. 1 and 2). Fig. 1 shows that the  $V_x$ -components are absent in model VTI-1 and ORT and nonzero in VTI-2. The zero and nonzero  $V_x$ -components of the numerical methods are very consistent with the analytical solutions with high accuracies. Fig. 2 shows that all the  $V_z$ -components are nonzero in three models and all the numerical solutions match well with the analytical ones. Comparing the rms errors, the three numerical methods yield accurate solutions for all the nonzero  $V_x$ - and  $V_z$ -components. One may also see that two recursive convolution methods (TS1-RC, TS2-RC) yield almost the same solutions and have slightly smaller errors than A-PDE.

Fig. 3 shows the numerical solutions of the  $V_z$ -components against the analytical solutions in TTI situations of the three models, where we maintained all the moduli but rotated the symmetry axes  $45^\circ$  clockwise, so that the discretized model parameters involve the tilted angle beside the moduli at every point in the models. These results indicate that three numerical methods generate very consistent results with the 3-D analytical wavefield solutions and verify their applicability to TTI media.

### B. Experiments of Parallel Computing

In the calibration experiment, 2.5-D modeling was performed using fully parallelized computing, employing the equivalent number of cores for wavenumber sampling. This setup represents the ideal modeling environment; however, the number of cores may need to be adjusted due to limitations in

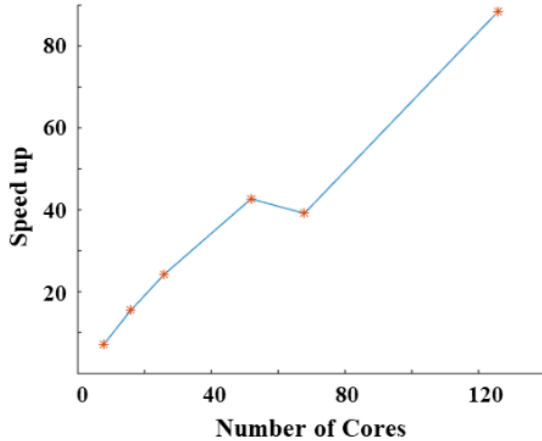


Fig. 4. Speed-up plot utilizing 8, 16, 26, 52, 68, and 126 cores. Speed-up is defined as the single core runtime divided by run time on parallel processing.

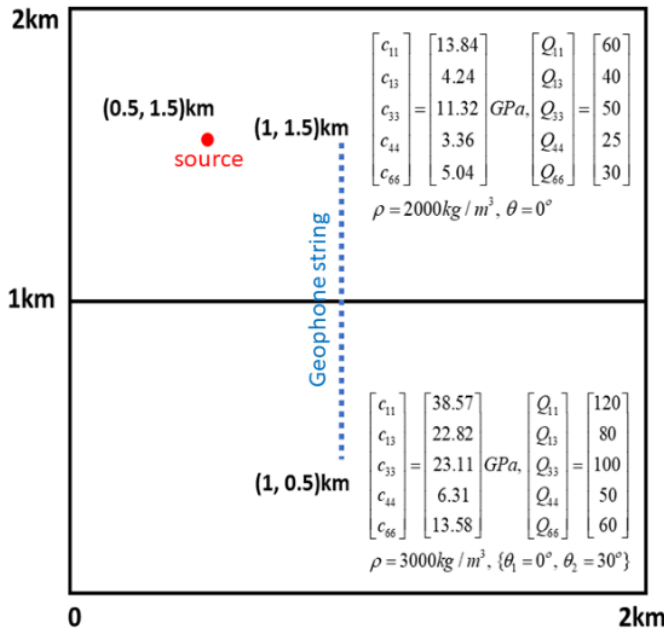


Fig. 5. Two-layered model. The upper layer is a viscoelastic VTI, and the lower layer is a viscoelastic VTI ( $\theta_0 = 0^\circ$ ) and a viscoelastic TTI ( $\theta_0 = 30^\circ$ ). The source is located on the (0.5, 1.5 km) overlying VTI layer, and receiver array is vertically aligned from 1.5 to 0.5 km with 25 m equal spacing.

computer equipment or a dense wavenumber scheme. We measured the speed-ups of runtimes in the VTI-2 homogeneous media under high attenuation conditions, using the same media as in the previous section with  $N_{ky} = 126$   $k_y$ -samples. The modeling was conducted using 8, 16, 26, 52, 68, and 126 cores on a high-performance computing (HPC) system equipped with  $2 \times$  Intel Xeon Gold 6230R 26-Core 2.1 GHz processors. The configurations with 26 and 52 cores represent the full utilization of one and two CPUs, respectively, while 68 and 126 cores represent half and full parallelization for wavenumber sampling. Fig. 4 illustrates the speed-ups in modeling runtime corresponding to the number of cores. Speed-up is defined as the runtime on a single core, which is 1693.8 min, divided by the runtimes of parallel computing. The speed-up plot exhibits an almost linear trend, except for the case of

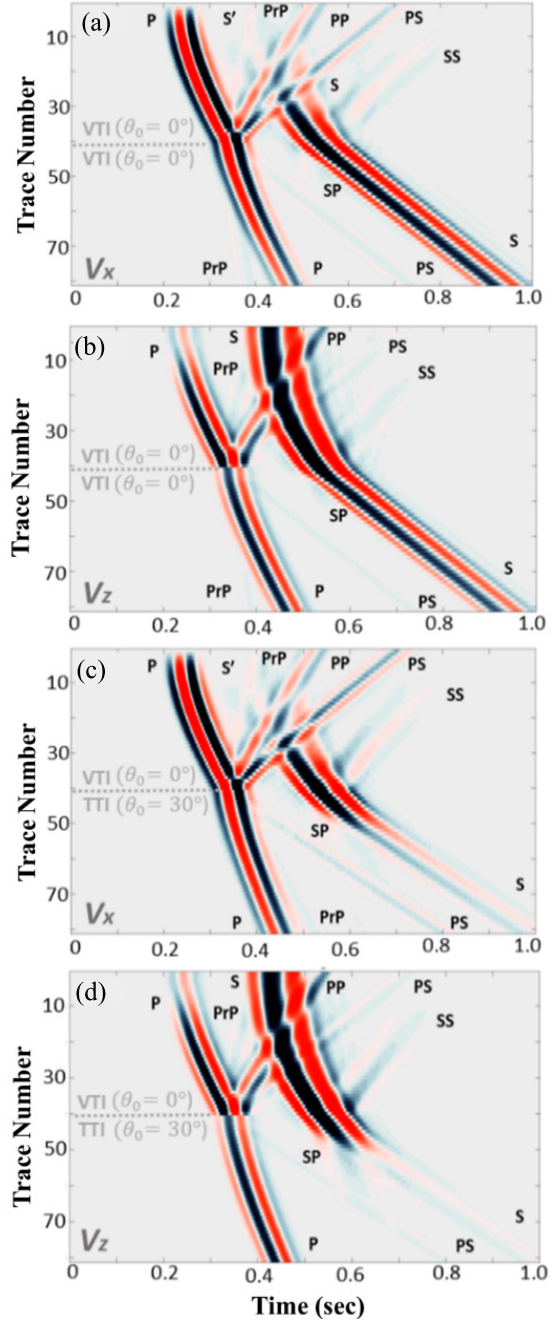


Fig. 6. Common shot gathers of (a) and (c) horizontal component and (b) and (d) vertical component in (a) and (b) VTI-VTI, and (c) and (d) VTI-TTI model shown in Fig. 5.

68 cores. The slower computation compared to 52 cores may result from the OpenMP/MPI application to the HPC system, as it is composed of two CPUs in each node. Meanwhile, fully parallelized computing achieves a nearly linear trend and is approximately 88 times faster than a single core. The memory storage exhibits a first-order linear relationship in the form of  $a + (N_{\text{core}} - 1)b$ , where  $a = 0.4$  Gb and  $b = 0.293$  Gb. The maximum memory occupation observed during fully parallelized computation is approximately 37 Gb.

### C. Two-Layered Model

To observe seismic wave behavior at the interface between two viscoelastic anisotropic media, we designed a vertical

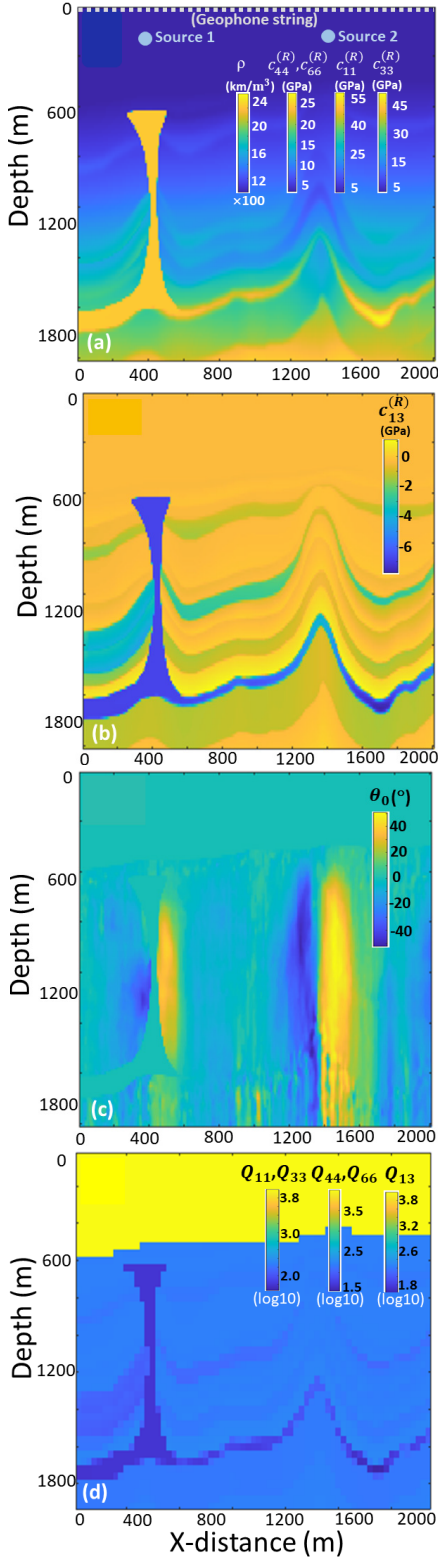


Fig. 7. (a) Density and relaxed moduli  $\{\rho, c_{1'1'}^{(R)}, c_{3'3'}^{(R)}, c_{4'4'}^{(R)}, c_{6'6'}^{(R)}\}$ . (b) Relaxed moduli  $\{c_{13}^{(R)}\}$ . (c) Tilted angle  $\{\theta_0\}$ . (d) Quality factors  $\{Q_{11}, Q_{13}, Q_{33}, Q_{44}, Q_{66}\}$  of BP2007-TTI model for 2.5-D wave modeling experiments. Two sources are located (450, 200 m) and (1350, 200 m) above the salt dome and anticline, respectively. A receiver array is horizontally aligned every 15 m from 150 to 1830 m at the same depth (200 m) over the two sources.

seismic profiling (VSP) for a two-layer viscoelastic anisotropic model (see Fig. 5). The upper layer is a viscoelastic

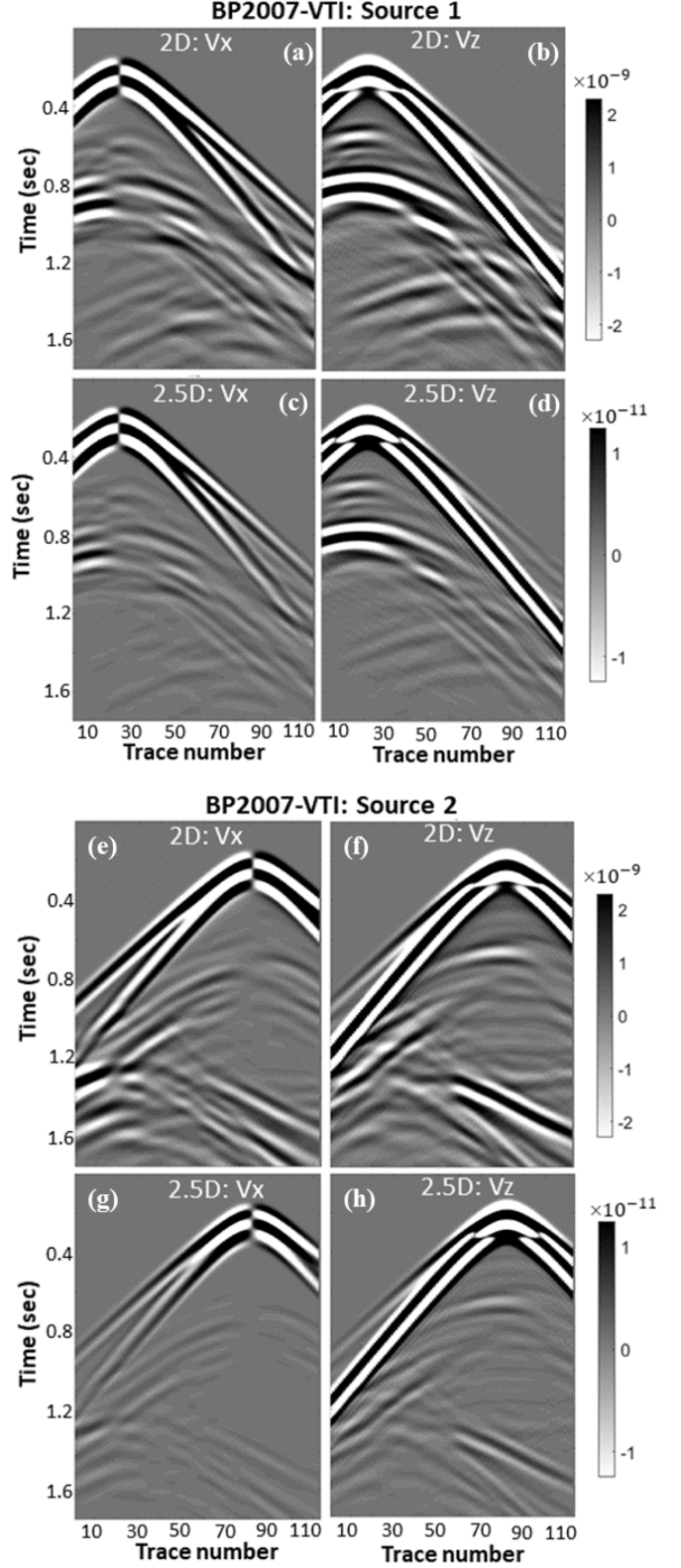


Fig. 8. Common shot gathers of (a) and (e) 2-D horizontal component, (b) and (f) 2-D vertical component, (c) and (g) 2.5-D horizontal component, and (d) and (h) 2.5-D vertical component using the TS2-RC method for BP2007-VTI model shown in Fig. 7 except for the tilted angle ( $\theta_0 = 0$  everywhere) by (a)–(d) source 1 over the salt dome (a)–(d) and (e)–(h) source 2 over the anticline.

VTI medium, and the lower layer has two situations: a stiffer VTI layer than the upper and a viscoelastic TTI medium.

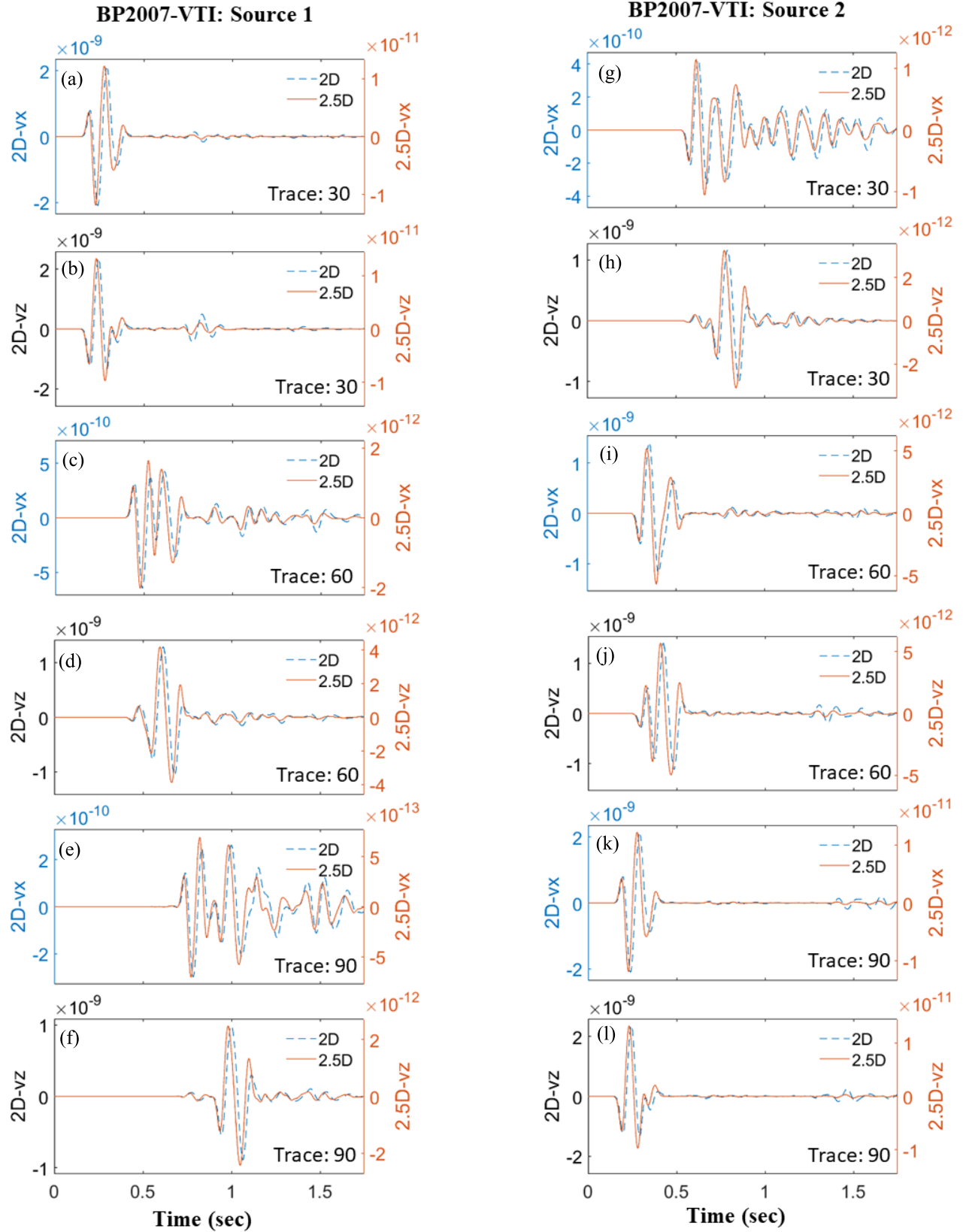


Fig. 9. Seismograms of three traces (no. 30, 60, and 90) of (a)–(f) source 1 and (g)–(l) source 2 in BP2007-VTI, Fig. 8. Three receivers are located on (a), (b), (g), and (h) (585, 0 m), (c), (d), (i), (j) (1035, 0 m), and (e), (f), (k), and (l) (1485, 0 m), respectively. Fig. 9 on (a), (c), (e), (g), (i), and (k) left column are the horizontal component, and (b), (d), (f), (h), (j), and (l) right column are the vertical component.

The model size is  $2 \times 2$  km, with a flat interface at a depth of 1 km. The subdomain size is  $25 \times 25$  m and discretized

by  $5 \times 5$  Chebyshev points. The source is positioned at (0.5, 1.5 km), and 81 receivers are aligned between (1, 0.5 km)

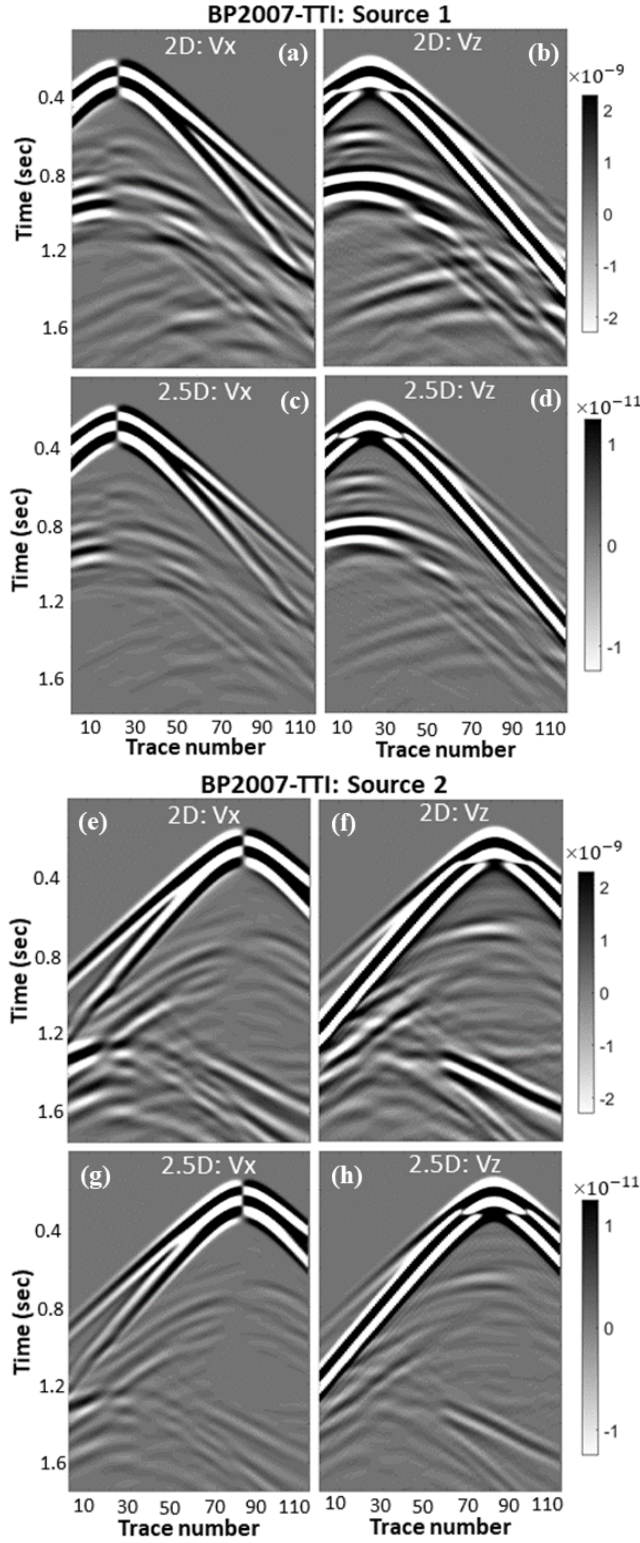


Fig. 10. Common shot gathers of (a) and (e) 2-D horizontal component, (b) and (f) 2-D vertical component, (c) and (g) 2.5-D horizontal component, and (d) and (h) 2.5-D vertical component using the TS2-RC method for BP2007-TTI model shown in Fig. 7 by (a)–(d) source 1 over the salt dome and (e)–(h) source 2 over the anticline.

and (1, 1.5 km) with equal spacing of 12.5 m. The source signal is the Ricker wavelet with a dominant frequency of  $f_c = 30$  Hz and a delay time of 0.05 s. The simulation consists of 10 000-time steps with a duration of 100  $\mu$ s.

Fig. 6 gives the common-shot gathers of the  $V_x$ - and  $V_z$ -components in two cases—the underlying VTI ( $\theta_0 = 0$ ) and TTI media ( $\theta_0 = 30^\circ$ ) medium. From these results, one can identify various phases of seismic waves due to the interface, e.g., the direct arrivals (P, S), refraction (PrP), reflections (PP, SS), and conversion (PS) are seen in the upper layer, and the transmissions (P, S), the transmitted conversion (PS, SP) are found in the lower layer. The significant differences between the underlying VTI and TTI media are also observed. The underlying TTI generates stronger reflections (PP, SS) and conversion (PS) in the upper layer for both components and much weaker transmission (S) in the lower layer than the underlying VTI layer. Additionally, the conversion SP in the lower layer is more pronounced compared to the underlying VTI layer.

#### D. BP2007-TTI Model

To demonstrate the capability of the proposed methods, a  $1.98 \times 1.98$  km BP2007-TTI model shown in Fig. 7 was employed. It has a salt dome and an anticline, originally including three elastic Thomsen's parameters:  $\{\alpha, \delta, \varepsilon\}$  and tilted angle  $\theta_0$  [see Fig. 7(c)]. Based on the given  $\alpha$ , we rescaled the density within the range 1000–2400 kg/m<sup>3</sup> and obtained the S-wave velocity  $\beta$  in terms of the empirical relationship  $\beta = \alpha/\sqrt{1.73}$ . Then, we transformed these Thomsen's parameters into the relaxed elastic moduli  $\{c_{1'1'}^{(R)}, c_{1'3'}^{(R)}, c_{3'3'}^{(R)}, c_{4'4'}^{(R)}, c_{6'6'}^{(R)}\}$  [see Fig. 7(a) and (b)] and complemented five independent quality factors given in Fig. 7(d). The model was divided by non-overlapping subdomains of  $30 \times 30$  m and each subdomain was sampled by  $5 \times 5$  Chebyshev points. Two sources are placed above the salt dome (450, 200 m) and the anticline (1350, 200 m). A geophone string is positioned horizontally every 15 m from 150 to 1830 m at the same depth (200 m) over the two sources [see Fig. 7(a)]. The source signal is a Ricker wavelet with a central frequency of 15 Hz and a time delay of 0.1 s. According to these model parameters and the source frequency, we found the cut-off wavenumber  $k_y^c = 0.4797$  and the number of the  $k_y$ -samples  $N_{ky} = 311$ . In order to see the difference in wavefield between the 2-D and 2.5-D, VTI and TTI media, we conducted the 2-D and 2.5-D wave modeling using the three methods A-PDE, TS1-RC, and TS2-RC for the BP2007-VTI [ $\theta_0 = 0$  everywhere in Fig. 7(c)] and BP2007-TTI model, respectively. One hundred fifty-six cores were utilized to achieve the parallel computing in the  $k_y$ -domain, and spent about 162 and 175 min for the two models. From the modeling results, we found that the three methods A-PDE, TS1-RC, and TS2-RC generate very similar seismograms. Hence, we only give the results yielded by the TS2-RC method for BP2007-VTI and -TTI models.

Fig. 8 displays the common-shot gathers of  $V_x$ - and  $V_z$ -components obtained by the 2-D and 2.5-D wave modeling for two sources in the model BP2007-VTI. From these results, one can clearly see three features: 1) the similar phases of all wave events (direct, reflected, and scattered waves) between 2-D and 2.5-D modeling except for a significant difference in amplitude, i.e., the magnitudes of the 2.5-D results are almost two order ( $10^{-2}$ ) less than those of the 2-D results; 2) the

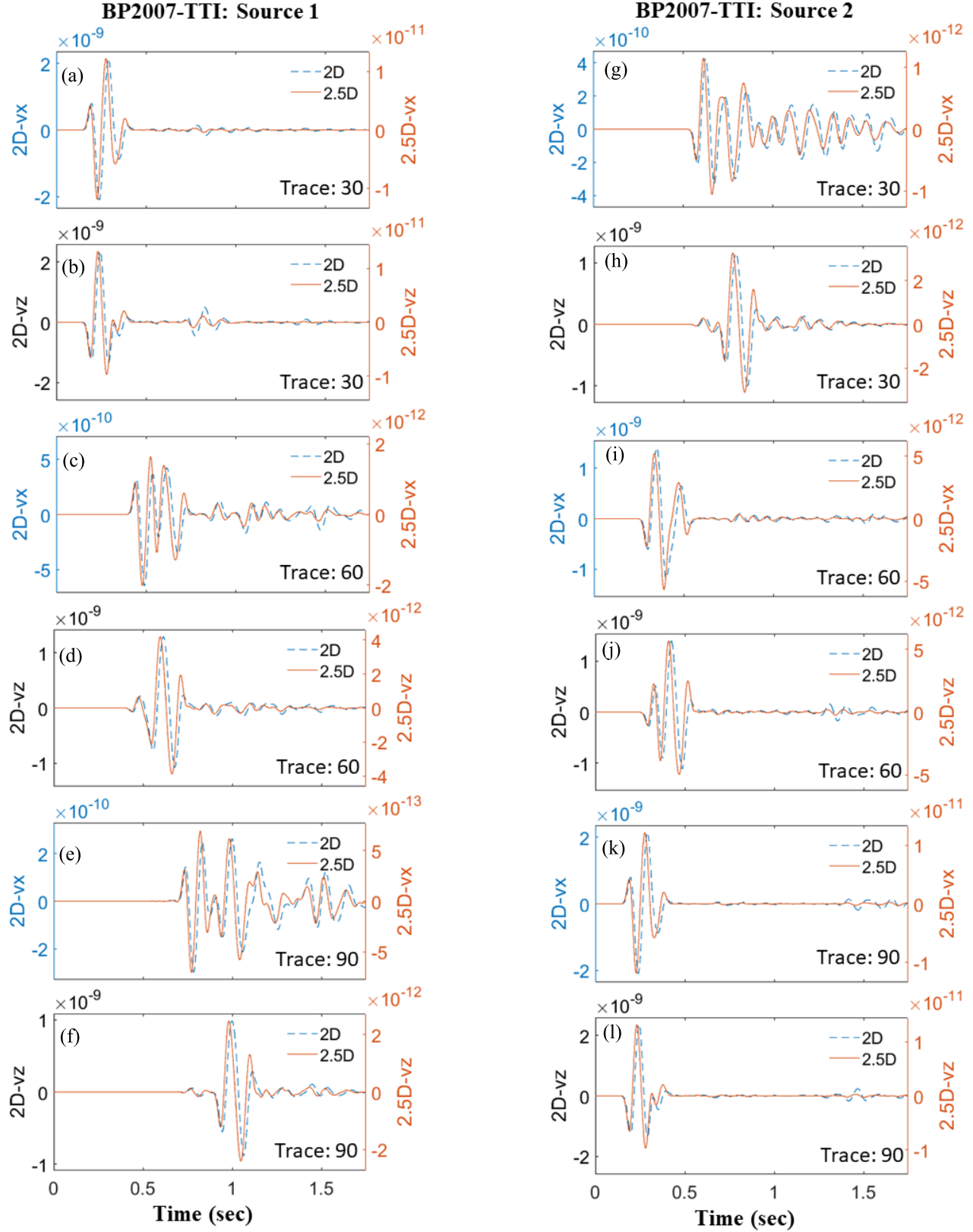


Fig. 11. Seismograms of three traces (no. 30, 60, and 90) of (a)–(f) source 1 and (g)–(l) source 2 in BP2007-TTI, Fig. 10. Three receivers are located on (a), (b), (g), and (h) (585, 0 m), (c), (d), (i), and (j) (1035, 0 m), and (e), (f), (k), and (l) (1485, 0 m), respectively. Fig. 11 on (a), (c), (e), (g), (i), and (k) left column are the horizontal component, and (b), (d), (f), (h), (j), and (l) right column are the vertical component.

results in the left panel of Fig. 8 exhibit strong reflections and scattering from the salt dome and weak reflections and scattering from the anticline because the source is just over

the salt dome; and 3) the results in Fig. 8(e)–(h) indicate strong reflections and scattering from the two buried geological structures as the source moves to just over the anticline.

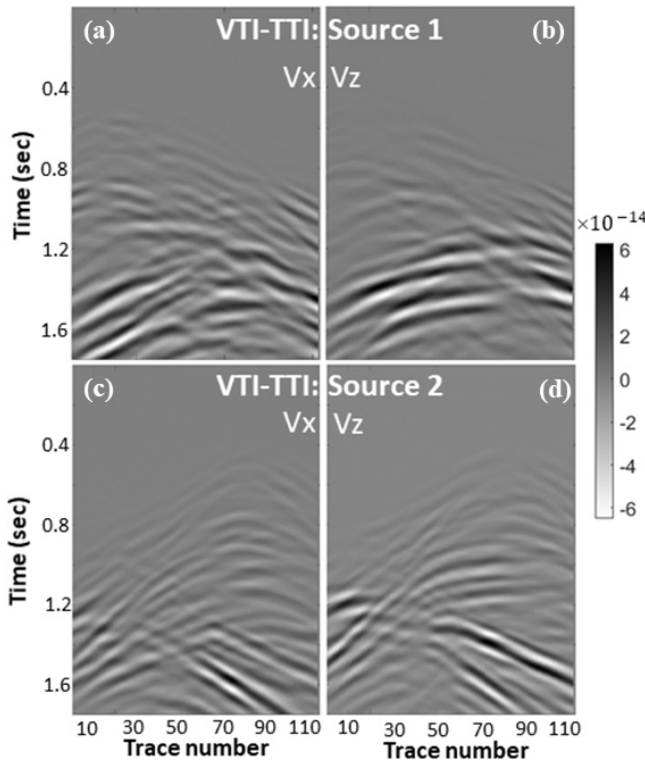


Fig. 12. Seismogram difference of the 2.5-D wave modeling (TSm-RC method) between BP2007-VTI and BP2007-TTI models. (a) Horizontal component difference source 1. (b) Vertical component difference source 1. (c) Horizontal component difference source 2. (d) Vertical component difference source 2.

To more clearly see the difference between the 2-D and 2.5-D modeling, we plotted Fig. 9 which shows the 2-D and 2.5-D seismograms of three traces (trace numbers are 30, 60, and 90) in Fig. 8. Fig. 9 clearly indicates the differences in not only their amplitudes but also the phase delays in two components between the line- and point-source generated wavefield.

Fig. 10 displays the common-shot gathers of  $V_x$ - and  $V_z$ -components yielded by the 2-D and 2.5-D wave modeling for the model BP2007-TTI. Compared with Fig. 8, one hardly sees the difference between the VTI and TTI models in these common-short gathers. Similar features shown in Fig. 8 to those shown in Fig. 10 may be attributed to the dominance of the dome and anticline structure, along with the variation in tilted angles in deep depth. Using the line-source (2-D) and the point-source (2.5-D) wave modeling both enable us to simulate the reflections and scatterings from the 2-D salt dome and the anticlines regardless of the differences in amplitude and phase delays. Fig. 11 gives the 2-D and 2.5-D seismograms of three traces in Fig. 10 and clearly indicate significant differences in not only their amplitude but also their phases in both  $V_x$ - and  $V_z$ -components. Fig. 12 shows the seismogram difference of the common-short gathers between BP2007-VTI and BP2007-TTI models, and clearly displays the significant differences in the deep reflections and scatterings due to the anticlines where the tilted angle  $\theta_0$  changes [see Fig. 7(c)]. This feature implies that the tilted angle  $\theta_0$  in the anticlines mainly affects the deep reflections and scatterings in this model, a little influence on the first arrivals and the shallow

reflections and scatterings because of the overlying VTI layers [see Fig. 7(c)].

#### IV. CONCLUSION

We have presented two numerical methods, A-PDE and TSm-RC, for the purpose of simulating 2.5-D seismic waves in arbitrary viscoelastic TTI media. These methods demonstrate greater practicality compared to conventional 2-D seismic wave modeling approaches. Notably, the TSm-RC method shows the potential for improved accuracy, while keeping computational memory and runtime requirements nearly identical to those of the A-PDE method.

In theory, we have provided the 2.5-D wave equations, which hold true for a wide range of viscoelastic anisotropic media, with a particular focus on viscoelastic TTI media that are frequently encountered in practical applications. From a technical standpoint, we have showcased the efficient solution of these 2.5-D wave equations through real-domain implementation and fully parallel computing techniques. This combined approach offers an efficient alternative for simulating the 3-D wavefield in diverse 2-D viscoelastic TTI media.

Our calibration experiments demonstrate that the numerical seismograms generated by the 2.5-D wave modeling align closely with analytical solutions, specifically in homogeneous VTI and TTI media. Furthermore, these experiments confirm that the TSm-RC ( $m \geq 1$ ) method provides more accurate solutions compared to the A-PDE method.

In our modeling experiments, we applied the proposed methods to a two-layered model and two benchmark complex geological models BP2007-VTI and BP2007-TTI. These experiments showcased the capabilities of our methods in generating 3-D wavefields within complex and heterogeneous 2-D viscoelastic anisotropic geological structures.

The TSm-RC method holds significant promise as a valuable tool for analyzing and characterizing seismic wave propagation in viscoelastic anisotropic media. It forms a fundamental component of seismic FWI techniques, which are widely applicable in subsurface imaging for natural resource exploration, seismological studies of Earth's interior, and geoengineering. These areas represent our ongoing research interests.

#### REFERENCES

- [1] J. M. Carcione, D. Kosloff, A. Behle, and G. Seriani, "A spectral scheme for wave propagation simulation in 3-D elastic-anisotropic media," *Geophysics*, vol. 57, no. 12, pp. 1593–1607, Dec. 1992, doi: [10.1190/1.1443227](https://doi.org/10.1190/1.1443227).
- [2] Z. Qiao, C. Sun, and D. Wu, "Theory and modelling of constant-Q viscoelastic anisotropic media using fractional derivative," *Geophys. J. Int.*, vol. 217, no. 2, pp. 798–815, Jan. 2019, doi: [10.1093/gji/ggz050](https://doi.org/10.1093/gji/ggz050).
- [3] N. Wang, G. Xing, T. Zhu, H. Zhou, and Y. Shi, "Propagating seismic waves in VTI attenuating media using fractional viscoelastic wave equation," *J. Geophys. Res., Solid Earth*, vol. 127, no. 4, Apr. 2022, Art. no. e2021JB023280, doi: [10.1029/2021jb023280](https://doi.org/10.1029/2021jb023280).
- [4] K. Aki and P. G. Richards, "Stress-strain relations and the strain-energy function," in *Quantitative Seismology*, J. Ellis, Ed., 2nd ed. Los Angeles, CA, USA: Univ. Science Books, 2002, pp. 20–23.
- [5] J. M. Carcione, D. Kosloff, and R. Kosloff, "Viscoacoustic wave propagation simulation in the Earth," *Geophysics*, vol. 53, no. 6, pp. 769–777, Jun. 1988, doi: [10.1190/1.1442512](https://doi.org/10.1190/1.1442512).

- [6] N. V. da Silva, G. Yao, and M. Warner, "Wave modeling in visco-acoustic media with transverse isotropy," *Geophysics*, vol. 84, no. 1, pp. C41–C56, Jan. 2019, doi: [10.1190/geo2017-0695.1](https://doi.org/10.1190/geo2017-0695.1).
- [7] J. M. Carcione and S. Picotti, "P-wave seismic attenuation by slow-wave diffusion: Effects of inhomogeneous rock properties," *Geophysics*, vol. 71, no. 3, pp. O1–O8, May 2006, doi: [10.1190/1.2194512](https://doi.org/10.1190/1.2194512).
- [8] P. Moczo and J. Kristek, "On the rheological models used for time-domain methods of seismic wave propagation," *Geophys. Res. Lett.*, vol. 32, no. 1, pp. 1–5, Jan. 2005, Art. no. L01306, doi: [10.1029/2004gl021598](https://doi.org/10.1029/2004gl021598).
- [9] L. Kai, C. Dan-Ping, H. Bing-Hong, and W. Guo-Chen, "Characterization for wave equations in viscoelastic media based on the constant Q property," *Appl. Geophys.*, vol. 17, no. 4, pp. 561–575, Dec. 2020, doi: [10.1007/s11770-020-0838-2](https://doi.org/10.1007/s11770-020-0838-2).
- [10] L. Auer, A. M. Nuber, S. A. Greenhalgh, H. Maurer, and S. Marelli, "A critical appraisal of asymptotic 3D-to-2D data transformation in full-waveform seismic crosshole tomography," *Geophysics*, vol. 78, no. 6, pp. R235–R247, Nov. 2013, doi: [10.1190/geo2012-0382.1](https://doi.org/10.1190/geo2012-0382.1).
- [11] Q. Yang, B. Zhou, M. K. Riahi, and M. Al-Khaleel, "Frequency-domain seismic data transformation from point source to line source for 2D viscoelastic anisotropic media," *Geophysics*, vol. 87, no. 2, pp. T85–T98, Dec. 2021, doi: [10.1190/geo2021-0166.1](https://doi.org/10.1190/geo2021-0166.1).
- [12] T. Forbriger, L. Groos, and M. Schäfer, "Line-source simulation for shallow-seismic data. Part 1: Theoretical background," *Geophys. J. Int.*, vol. 198, no. 3, pp. 1387–1404, Jul. 2014, doi: [10.1093/gji/ggu199](https://doi.org/10.1093/gji/ggu199).
- [13] M. Schäfer, L. Groos, T. Forbriger, and T. Bohlen, "Line-source simulation for shallow-seismic data. Part 2: Full-waveform inversion—A synthetic 2-D case study," *Geophys. J. Int.*, vol. 198, no. 3, pp. 1405–1418, Jul. 2014, doi: [10.1093/gji/ggu171](https://doi.org/10.1093/gji/ggu171).
- [14] Z. Song and P. R. Williamson, "Frequency-domain acoustic-wave modeling and inversion of crosshole data: Part I—2.5-D modeling method," *Geophysics*, vol. 60, no. 3, pp. 784–795, May 1995, doi: [10.1190/1.1443817](https://doi.org/10.1190/1.1443817).
- [15] P. R. Williamson and R. G. Pratt, "A critical review of acoustic wave modeling procedures in 2.5 dimensions," *Geophysics*, vol. 60, no. 2, pp. 591–595, Mar. 1995, doi: [10.1190/1.1443798](https://doi.org/10.1190/1.1443798).
- [16] J. R. Ernst, A. G. Green, H. Maurer, and K. Holliger, "Application of a new 2D time-domain full-waveform inversion scheme to crosshole radar data," *Geophysics*, vol. 72, no. 5, pp. J53–J64, Sep. 2007, doi: [10.1190/1.2761848](https://doi.org/10.1190/1.2761848).
- [17] L. Auer, A. M. Nuber, S. A. Greenhalgh, H. Maurer, and S. Marelli, "A critical appraisal of asymptotic 3D-to-2D data transformation in full-waveform seismic crosshole tomography," *Geophysics*, vol. 78, no. 6, pp. R235–R247, Nov. 2013, doi: [10.1190/geo2012-0382.1](https://doi.org/10.1190/geo2012-0382.1).
- [18] B. Zhou, S. Greenhalgh, and H. Maurer, "2.5-D frequency-domain seismic wave modeling in heterogeneous, anisotropic media using a Gaussian quadrature grid technique," *Comput. Geosci.*, vol. 39, pp. 18–33, Feb. 2012, doi: [10.1016/j.cageo.2011.06.005](https://doi.org/10.1016/j.cageo.2011.06.005).
- [19] S.-B. Yang, B. Zhou, and C.-Y. Bai, "A generalized 2.5-D time-domain seismic wave equation to accommodate various elastic media and boundary conditions," *Pure Appl. Geophys.*, vol. 178, no. 8, pp. 2999–3025, Jun. 2021, doi: [10.1007/s00024-021-02775-2](https://doi.org/10.1007/s00024-021-02775-2).
- [20] Q. Yang, B. Zhou, M. K. Riahi, and M. Al-khaleel, "A new generalized stiffness reduction method for 2D/2.5D frequency-domain seismic wave modeling in viscoelastic anisotropic media," *Geophysics*, vol. 85, no. 6, pp. T315–T329, Nov. 2020, doi: [10.1190/geo2020-0143.1](https://doi.org/10.1190/geo2020-0143.1).
- [21] S. M. Day and J. B. Minster, "Numerical simulation of attenuated wavefields using a Padé approximant method," *Geophys. J. Int.*, vol. 78, no. 1, pp. 105–118, Jul. 1984, doi: [10.1111/j.1365-246x.1984.tb06474.x](https://doi.org/10.1111/j.1365-246x.1984.tb06474.x).
- [22] J. M. Carcione, D. Kosloff, and R. Kosloff, "Wave propagation simulation in a linear viscoelastic medium," *Geophys. J. Int.*, vol. 95, no. 3, pp. 597–611, Dec. 1988, doi: [10.1111/j.1365-246x.1988.tb06706.x](https://doi.org/10.1111/j.1365-246x.1988.tb06706.x).
- [23] T. Bai, I. Tsvankin, and X. Wu, "Waveform inversion for attenuation estimation in anisotropic media," *Geophysics*, vol. 82, no. 4, pp. WA83–WA93, Jul. 2017, doi: [10.1190/geo2016-0596.1](https://doi.org/10.1190/geo2016-0596.1).
- [24] J. O. Blanch, J. O. A. Robertsson, and W. W. Symes, "Modeling of a constant Q: Methodology and algorithm for an efficient and optimally inexpensive viscoelastic technique," *Geophysics*, vol. 60, no. 1, pp. 176–184, Jan. 1995, doi: [10.1190/1.1443744](https://doi.org/10.1190/1.1443744).
- [25] H. Emmerich and M. Korn, "Incorporation of attenuation into time-domain computations of seismic wave fields," *Geophysics*, vol. 52, no. 9, pp. 1252–1264, Sep. 1987, doi: [10.1190/1.1442386](https://doi.org/10.1190/1.1442386).
- [26] Q. Hao and S. Greenhalgh, "The generalized standard-linear-solid model and the corresponding viscoacoustic wave equations revisited," *Geophys. J. Int.*, vol. 219, no. 3, pp. 1939–1947, Sep. 2019, doi: [10.1093/gji/ggz407](https://doi.org/10.1093/gji/ggz407).
- [27] Q. Hao and S. Greenhalgh, "Nearly constant Q models of the generalized standard linear solid type and the corresponding wave equations," *Geophysics*, vol. 86, no. 4, pp. T239–T260, Jul. 2021, doi: [10.1190/geo2020-0548.1](https://doi.org/10.1190/geo2020-0548.1).
- [28] J. O. A. Robertsson, "A numerical free-surface condition for elastic-viscoelastic finite-difference modeling in the presence of topography," *Geophysics*, vol. 61, no. 6, pp. 1921–1934, Nov. 1996, doi: [10.1190/1.1444107](https://doi.org/10.1190/1.1444107).
- [29] P. Moczo, J. O. A. Robertsson, and L. Eisner, "The finite-difference time-domain method for modeling of seismic wave propagation," in *Advances in Geophysics*, vol. 48, R.-S. Wu, V. Maupin, and R. Dmowska, Eds. Amsterdam, The Netherlands: Elsevier, Jun. 2007, pp. 421–516.
- [30] T. Zhu and J. M. Harris, "Modeling acoustic wave propagation in heterogeneous attenuating media using decoupled fractional Laplacians," *Geophysics*, vol. 79, no. 3, pp. T105–T116, May 2014, doi: [10.1190/geo2013-0245.1](https://doi.org/10.1190/geo2013-0245.1).
- [31] J. Sun, T. Zhu, and S. Fomel, "Viscoacoustic modeling and imaging using low-rank approximation," *Geophysics*, vol. 80, no. 5, pp. A103–A108, Sep. 2015, doi: [10.1190/geo2015-0083.1](https://doi.org/10.1190/geo2015-0083.1).
- [32] J. Yang and H. Zhu, "A time-domain complex-valued wave equation for modelling visco-acoustic wave propagation," *Geophys. J. Int.*, vol. 215, no. 2, pp. 1064–1079, Aug. 2018, doi: [10.1093/gji/ggy323](https://doi.org/10.1093/gji/ggy323).
- [33] J. Yang, H. Zhu, X. Li, L. Ren, and S. Zhang, "Estimating P wave velocity and attenuation structures using full waveform inversion based on a time domain complex-valued viscoacoustic wave equation: The method," *J. Geophys. Res. Solid Earth*, vol. 125, no. 6, Jun. 2020, Art. no. e2019JB019129, doi: [10.1029/2019jb019129](https://doi.org/10.1029/2019jb019129).
- [34] N. Wang, T. Zhu, H. Zhou, H. Chen, X. Zhao, and Y. Tian, "Fractional Laplacians viscoacoustic wavefield modeling with k-space-based time-stepping error compensating scheme," *Geophysics*, vol. 85, no. 1, pp. T1–T13, Jan. 2020, doi: [10.1190/geo2019-0151.1](https://doi.org/10.1190/geo2019-0151.1).
- [35] R. Luebbers, F. P. Hunsberger, K. S. Kunz, R. B. Standler, and M. Schneider, "A frequency-dependent finite-difference time-domain formulation for dispersive materials," *IEEE Trans. Electromagn. Compat.*, vol. 32, no. 3, pp. 222–227, Aug. 1990, doi: [10.1109/15.57116](https://doi.org/10.1109/15.57116).
- [36] D. F. Kelley and R. J. Luebbers, "Piecewise linear recursive convolution for dispersive media using FDTD," *IEEE Trans. Antennas Propag.*, vol. 44, no. 6, pp. 792–797, Jun. 1996, doi: [10.1109/8.509882](https://doi.org/10.1109/8.509882).
- [37] N. Cheng, A. C. Cheng, and M. N. Toksoz, "A time-domain finite-difference method with attenuation by a recursive algorithm," Earth Resour. Lab., Massachusetts Inst. Technol., Cambridge, MA, USA, Tech. Rep. 1996-12, 1996.
- [38] J. Bielak, H. Karaoglu, and R. Taborda, "Memory-efficient displacement-based internal friction for wave propagation simulation," *Geophysics*, vol. 76, no. 6, pp. T131–T145, Nov. 2011, doi: [10.1190/geo2011-0019.1](https://doi.org/10.1190/geo2011-0019.1).
- [39] B. Zhou, M. Won, and C. Jin, "New numerical schemes for time-domain seismic wave modeling in viscoelastic media," presented at the 2nd Int. Meeting Appl. Geosci. Energy, 2022.
- [40] C. Jin, B. Zhou, S. Greenhalgh, M. Won, M. Riahi, and M. Zemerly, "Generalized recursive convolution method for viscoelastic wave modeling," in *Proc. 84th EAGE Annu. Conf. Exhib.*, no. 1. Vienna, Austria: European Association of Geoscientists & Engineers, Jun. 2023, pp. 1–5.
- [41] R. E. Sheriff and L. P. Geldart, "Anisotropic media," in *Exploration Seismology*, 2nd ed. Cambridge, U.K.: Cambridge Univ. Press, 1995, pp. 33–72.
- [42] L. Thomsen, "Weak elastic anisotropy," *Geophysics*, vol. 51, no. 10, pp. 1954–1966, Oct. 1986.
- [43] Y. Zhu and I. Tsvankin, "Plane-wave propagation in attenuative transversely isotropic media," *Geophysics*, vol. 71, no. 2, pp. T17–T30, Mar. 2006, doi: [10.1190/1.2187792](https://doi.org/10.1190/1.2187792).
- [44] T. Bai and I. Tsvankin, "Time-domain finite-difference modeling for attenuative anisotropic media," *Geophysics*, vol. 81, no. 2, pp. C69–C77, Mar. 2016, doi: [10.1190/geo2015-0424.1](https://doi.org/10.1190/geo2015-0424.1).
- [45] T. Zhu, "Numerical simulation of seismic wave propagation in viscoelastic-anisotropic media using frequency-independent Q wave equation," *Geophysics*, vol. 82, no. 4, pp. WA1–WA10, Jul. 2017, doi: [10.1190/geo2016-0635.1](https://doi.org/10.1190/geo2016-0635.1).

- [46] Z. Qiao, C. Sun, and J. Tang, "Modelling of viscoacoustic wave propagation in transversely isotropic media using decoupled fractional Laplacians," *Geophys. Prospecting*, vol. 68, no. 8, pp. 2400–2418, Oct. 2020, doi: [10.1111/1365-2478.13006](https://doi.org/10.1111/1365-2478.13006).
- [47] B. Gu, S. Zhang, P. Duan, J. Huang, and J. Han, "Viscoacoustic wave equation for qP-wave in transversely isotropic media," *J. Appl. Geophys.*, vol. 203, Aug. 2022, Art. no. 104681, doi: [10.1016/j.jappgeo.2022.104681](https://doi.org/10.1016/j.jappgeo.2022.104681).
- [48] D. Komatitsch, C. Barnes, and J. Tromp, "Simulation of anisotropic wave propagation based upon a spectral element method," *Geophysics*, vol. 65, no. 4, pp. 1251–1260, Jul. 2000, doi: [10.1190/1.1444816](https://doi.org/10.1190/1.1444816).
- [49] J. Carcione, "Dynamical equations," in *Wave Fields in Real Media: Theory and Numerical Simulation of Wave Propagation in Anisotropic, Anelastic, Porous and Electromagnetic Media*, 2nd ed. London, U.K.: Elsevier, 2007, pp. 4–9.
- [50] É. Blanc, D. Komatitsch, E. Chaljub, B. Lombard, and Z. Xie, "Highly accurate stability-preserving optimization of the zener viscoelastic model, with application to wave propagation in the presence of strong attenuation," *Geophys. J. Int.*, vol. 205, no. 1, pp. 427–439, Feb. 2016, doi: [10.1093/gji/ggw024](https://doi.org/10.1093/gji/ggw024).
- [51] X. Liu, S. Greenhalgh, B. Zhou, and G. Heinson, "Generalized poro-viscoelastic model based on effective biot theory and its application to borehole guided wave analysis," *Geophys. J. Int.*, vol. 207, no. 3, pp. 1472–1483, Jul. 2016, doi: [10.1093/gji/ggw345](https://doi.org/10.1093/gji/ggw345).
- [52] B. Zhou, S. Greenhalgh, and M. Greenhalgh, "Wavenumber sampling strategies for 2.5-D frequency-domain seismic wave modelling in general anisotropic media," *Geophys. J. Int.*, vol. 188, no. 1, pp. 223–238, Jan. 2012, doi: [10.1111/j.1365-246X.2011.05246.x](https://doi.org/10.1111/j.1365-246X.2011.05246.x).
- [53] Q. Yang, B. Zhou, M. Engsig, M. K. Riahi, M. Al-Khaleel, and S. Greenhalgh, "Numerical Fréchet derivatives of the displacement tensor for 2.5-D frequency-domain seismic full-waveform inversion in viscoelastic TTI media," Dec. 2022, *arXiv:2212.04086*.
- [54] B. Zhou, G. Heinson, and A. Rivera-Rios, "Subdomain Chebyshev spectral method for 2D and 3D numerical differentiations in a curved coordinate system," *J. Appl. Math. Phys.*, vol. 3, no. 3, pp. 358–370, Mar. 2015, doi: [10.4236/jamp.2015.33047](https://doi.org/10.4236/jamp.2015.33047).
- [55] J. C. Butcher, "Linear multistep methods," in *Numerical Methods for Ordinary Differential Equations*, 2nd ed. West Sussex, U.K.: Wiley, 2008, pp. 105–113.
- [56] B. Zhou, M. Won, S. Greenhalgh, and X. Liu, "Generalized stiffness reduction method to remove the artificial edge-effects for seismic wave modelling in elastic anisotropic media," *Geophys. J. Int.*, vol. 220, no. 2, pp. 1394–1408, Feb. 2020, doi: [10.1093/gji/ggz529](https://doi.org/10.1093/gji/ggz529).
- [57] V. Vavryčuk, "Asymptotic Green's function in homogeneous anisotropic viscoelastic media," *Proc. Roy. Soc. A, Math., Phys. Eng. Sci.*, vol. 463, no. 2086, pp. 2689–2707, Jul. 2007, doi: [10.1098/rspa.2007.1862](https://doi.org/10.1098/rspa.2007.1862).



**Moosoo Won** was born in Winnipeg, MB, Canada, in 1990. He received the B.S. degree in earth system science from Yonsei University, Seoul, Republic of Korea, in 2016, and the M.S. degree in earth sciences from Khalifa University, Abu Dhabi, United Arab Emirates, in 2019, where he is currently pursuing the Ph.D. degree.



**Bing Zhou** received the Ph.D. in geophysics from the University of Adelaide, Adelaide, SA, Australia, in 1998.

He is an Associate Professor at the Department of Earth Science, Khalifa University of Science and Technology, Abu Dhabi, United Arab Emirates, an Adjunct Associate Professor at the Université du Québec en Abitibi-Témiscamingue, Rouyn-Noranda, QC, Canada. He is also Research Consultants of King Abdulaziz City for Science and Technology in Saudi Arab and ZZ-resistivity Imaging Company in Australia.

Dr. Zhou is an Associate Editor for *Near Surface Geophysics* and *Journal of Geophysics and Engineering*.



**Xu Liu** received the Ph.D. in geophysics from the University of Adelaide, Adelaide, SA, Australia.

He joined CIPR/KFUPM, Dhahran, Saudi Arabia, as a Research Scientist. His research interests include numerical modeling of seismic waves in reservoirs, seismic, magnetotelluric data processing and inversion, resistivity, and IP inversion.



**Mohamed Jamal Zemerly** (Senior Member, IEEE) received the M.Sc. degree from the University College Cardiff, Wales, U.K., in 1986, and Ph.D. degree from The University of Birmingham, Birmingham, U.K., in 1989. Since then, he worked at various U.K. universities, such as UCL, London, U.K., Warwick, Coventry, U.K., and Westminster, London, and then moved to Khalifa University, Abu Dhabi, United Arab Emirates, in summer 2000, where he is currently an Associate Professor (and ex-Computer Engineering Program Chair) at the Electrical Engineering and Computer Science Department.



**Mohammad Al-Khaleel** received the M.Sc. and Ph.D. degrees in applied mathematics (numerical analysis and scientific computing) from McGill University, Montreal, QC, Canada, in 2003 and 2007, respectively.

In 2007, he became an Assistant Professor of mathematics with the Department of Mathematics, Yarmouk University, Jordan, and afterward was promoted to an Associate Professor. He is currently an Associate Professor with the Department of Mathematics, Khalifa University, Abu Dhabi, United Arab Emirates. His research is of a multidisciplinary nature but the bulk of it has revolved around developing and implementing efficient and parallel numerical methods as well as analytical methods for solving differential equations (ordinary, partial, and fractional) that appear in many applications in different fields including seismic waves, nanofluid and microfluid dynamics, circuit simulations, and many others. He has also research interest in other areas of mathematics including topics in metric fixed point theory, fractional calculus, numerical parameter optimization, inverse and control problems, and the mathematical background of computer arithmetic circuits.



**Mohamed Kamel Riahi** earned the Ph.D. in applied mathematics from Pierre et Marie Curie University, Paris, France.

He has worked as a Post-Doctoral Research Associate with the Department of Mathematical Sciences, New Jersey Institute of Technology, Newark, NJ, USA, and at INRIA-Saclay Palaiseau France, Palaiseau, France, as a Post-Doctoral Researcher, with DeFI Team. He is currently assistant Professor of mathematics at the Khalifa University of Science and Technology, Abu Dhabi, United Arab Emirates.

He is an expert in scientific computing and numerical analysis related to partial differential equations. His research includes and is not limited to: space-time-domain decomposition methods, finite element method, integral equations method, numerical optimization, iterative method, preconditioning technique, shape optimization, optimal control problem, high-performance computing, and parallel programming.